Abundances and morphotypes of the coccolithophore *Emiliania huxleyi* in southern Patagonia compared to neighboring oceans and northern-hemisphere fjords

Francisco Díaz-Rosas[1,2], Catharina Alves-de-Souza[3], Emilio Alarcón[4,5], Eduardo Menschel[5,6], Humberto E. González[5,6], Rodrigo Torres[4,5], and Peter von Dassow[1,2]

[1] Facultad de Ciencias Biológicas, Departamento de Ecología, Pontificia Universidad Católica de Chile, Santiago, Chile.
[2] Instituto Milenio de Oceanografía de Chile, Concepción, Chile.
[3] Algal Resources Collection, MARBIONC, Center for Marine Science, University of North Carolina Wilmington, Wilmington, USA
[4] Centro de Investigación en Ecosistemas de la Patagonia, Coyhaique, Chile
[5] Centro de Investigación Dinámica de Ecosistemas Marinos de Altas Latitudes, Punta Arenas, Chile
[6] Instituto de Ciencias Marinas y Limnológicas, Universidad Austral de Chile, Valdivia, Chile.

Correspondence to: Francisco Díaz-Rosas (fdiazrosas7@gmail.com), Peter von Dassow (pvondassow@bio.puc.cl)

Abstract. Coccolithophores are potentially affected by ongoing ocean acidification, where rising CO_2 lowers seawater pH and calcite saturation state (Ω_{cal}). Southern Patagonian fjords and channels provide natural laboratories for studying these issues due to high variability in physical and chemical conditions. We surveyed coccolithophore assemblages in Patagonian fjords during late-spring 2015 and early-spring 2017. Surface Ω_{cal} exhibited large variations driven mostly by freshwater inputs. High Ω_{cal} conditions (max. 3.6) occurred in the Archipelago Madre de Dios. Ω_{cal} ranged from 2.0-2.6 in the western Strait of Magellan, 1.5-2.2 in the Inner Channel, and was sub-saturating (0.5) in Skyring Sound. *Emiliania huxleyi* was the only coccolithophore widely distributed in Patagonian fjords (> 96% of total coccolitophores), only disappearing in the Skyring Sound, a semi-closed mesohaline system. Correspondence analysis associated higher *E. huxleyi* biomasses with lower diatom biomasses. The highest *E. huxleyi* abundances in Patagonia were in the lower range of those reported in Norwegian fjords. Predominant morphotypes were distinct from those previously documented in nearby oceans but similar to those of Norwegian fjords. Moderate-calcified forms of *E. huxleyi* A morphotype were uniformly distributed throughout Patagonia fjords. The exceptional R/hyper-calcified coccoliths, associated with low Ω_{cal} values in Chilean and Peruvian coastal upwellings, were a minor component associated with high Ω_{cal} levels in Patagonia. Outlying mean index (OMI) niche analysis suggested that pH/Ω_{cal} conditions explained most variation in the realized niches of *E. huxleyi* morphotypes. The moderate-calcified A morphotype exhibited the widest niche-breadth (generalist), while the R/hyper-calcified morphotype exhibited a more restricted realized niche (specialist). Nevertheless, when considering an expanded sampling domain, including nearby Southeast Pacific coastal and offshore waters, even the R/hyper-calcified morphotype exhibited a higher niche breadth than other closely phylogenetically-related coccolithophore species. The occurrence of *E. huxleyi* in naturally low pH/Ω_{cal} environments indicates that its ecological response is plastic and capable of adaptation.

1 Introduction

Coccolithophores are small unicellular phytoplankton (3-30 µm) bearing intricate plates called coccoliths formed of calcite, the more stable form of calcium carbonate ($CaCO_3$) (Monteiro et al., 2016). Coccolithophores can carry out a substantial portion of $CaCO_3$ precipitation in pelagic systems (Broecker and Clark, 2009), which may enhance organic matter export by $CaCO_3$ ballasting (Klaas and Archer, 2002), while also lowering alkalinity (Zondervan et al., 2001) and contributing to the carbonate counter pump (Passow and Carlson, 2012). Thus, understanding how coccolithophores respond to environmental stressors, such as ocean acidification (OA) due to rising pCO_2, is necessary for predicting future ocean biogeochemistry.

Chemically, calcite stability in seawater can be parametrized using its saturation state, defined as $\Omega_{cal} = [Ca^{2+}] \cdot [CO_3^{2-}]/Ksp_{cal}$ (where Ksp_{cal} is the solubility constant for calcite), which is decreased by OA. When $\Omega_{cal} < 1$, calcite dissolution is thermodynamically favored, whereas calcite precipitation is favored when $\Omega_{cal} > 1$. Most of the ocean surface is predicted to remain supersaturated with respect to calcite in the future ocean (Feely et al., 2009), although some coastal zones may experience $\Omega_{cal} < 1$ in the euphotic zone either due to increased pCO_2 in areas of naturally high CO_2 upwelling (e.g., Franco et al., 2018) or due to freshening (e.g., Tynan et al., 2014). Furthermore, drops in Ω_{cal} may negatively affect biological calcite production rates even before becoming undersaturated (Doney et al., 2009).

In contrast to other calcifying organisms, coccolith formation occurs intracellularly in Golgi-derived vesicles, involving sustained fluxes of Ca^{2+} and dissolved inorganic carbon (primarily HCO_3^-) from the external medium, and high H^+ efflux to maintain cellular pH homeostasis (reviewed by Taylor et al., 2017). Which extracellular carbonate chemistry parameter most influences intracellular coccolithophore calcification is debated, e.g., whether Ωcal, or more complex relationships involving HCO_3^-, H^+, and CO_2 (Bach et al., 2015; Cyronak et al., 2016; Kottmeier et al., 2016; Gafar et al., 2018). Additionally, OA can have contrasting effects, with increased CO_2 availability potentially benefiting photosynthesis but high H^+ negatively affecting metabolisms besides calcification (Kottmeier et al., 2016; Paul and Bach, 2020). A wide range of calcification and growth responses to OA have been reported in laboratory studies of coccolithophores, mostly using the cosmopolitan and most abundant species *Emiliania huxleyi* (reviewed in Meyer and Riebesell, 2015). With some notable exceptions (e.g., Iglesias-Rodriguez et al., 2008), most culture studies showed reduced calcification rates of *E. huxleyi* in response to simulated OA, while there is no clear trend on growth rates. In a mesocosm experiment using a Norwegian fjord community, increased pCO_2 levels (> 500 µatm) resulted in lower growth rates of *E. huxleyi*, preventing it from blooming (Riebesell et al., 2017). This result contrasted with a long-term observational study showing a steady increase in coccolithophore stocks (related to diatoms and dinoflagellates) from pre-industrial to present-day high pCO_2 levels in the North Atlantic (Rivero-Calle et al., 2015), although both studies predict a decrease in net calcification.

Morphological variability in *E. huxleyi* has been reported with several morphotypes described so far with different degrees of calcification of the coccoliths, such as fusion of coccolith elements or calcite overgrowth (Young et al., 2003). Morphotype A coccoliths have a grill central area and tend to be moderately calcified, while morphotypes B and C have more lightly calcified distal shield elements and the central area is either a plate or open (type O) (Young and Westbroek, 1991; Hagino et al., 2011).

Additional morphotypes, or morphotype sub-classes, include B/C (intermediate in coccolith size between B and C) and R (*Reticulofenstra*-like), considered an A morphotype where distal shield elements are mostly or completely fused (Hagino et al., 2011). However, the readily identifiable qualitative distinctions may not easily translate into quantitative differences in the calcite produced per cell in the ecosystem, as for example, due to variability in the rate of coccoliths produced per cell (Johnsen and Bollmann, 2020).

Nevertheless, cultured isolates maintain their morphotype classifications even under variable environmental conditions that can alter total calcite production and even lead to coccolith malformation (e.g., Young and Westbroek, 1991; Langer et al., 2011; Müller et al., 2015; von Dassow et al., 2018; Mella-Flores et al., 2018), suggesting a genetic determination of coccolith morphology. One genetic marker has been associated with morphological variability in *E. huxleyi*. The calcium-binding protein GPA has been potentially associated with *E. huxleyi* coccolith deposition (Corstjens et al., 1998). Although the function of this protein is unclear, the 3' untranslated region (non-coding) showed consistent differences between morphotypes with all morphotypes A and R showing alleles (coccolith morphology motifs) CMM I, III, or IV and B, B/C and C morphotypes showing CMM II (Schroeder et al., 2005; Krueger-Hadfield et al., 2014). The uronic acid content of coccolith-associated polysaccharides also varies among strains, and the one R morphotype tested was much higher in this character than most of the other A morphotypes (Rickaby et al., 2016). It is likely that further comparative biochemical analyses following Rickaby et al. (2016) and/or associating comparative genomics analyses (e.g., studies such as Read et al., 2013; von Dassow et al., 2015; Bendif et al., 2019) with morphometric analyses may identify genetic markers associated with sub-types within the broader A and B. However, mitochondrial phylogenies classify *E. huxleyi* into a warmer-water clade and a colder water clade, and each clade contains both A (including R) morphotypes and B (or B/C or O) morphotypes (Hagino et al., 2011; Bendif et al., 2014), and B/C morphotypes also occurred in different genetic groups defined by microsatellite markers (Krueger-Hadfield et al., 2014), although another microsatellite study did find a separation between A and B/C morphotypes (Cook et al. 2013). Therefore, different morphologies likely correspond to stable genetically determined phenotypes that might reflect adaptations selected to specific conditions within a taxon whose recent evolution has been as a single biological species (Filatov, 2019).

In a global survey, Beaufort et al. (2011) found a general pattern of decreasing calcification with increasing pCO_2 and a concomitant decrease in CO_3^{2-}. Interestingly, calcite mass variability was predominantly the result of assemblage shifts both among closely related species and among morphotypes of the same species, from predominance of large and heavily-calcified *Gephyrocapsa oceanica* cells, through intermediate moderate-calcified *E. huxleyi* (A morphotype), to more lightly-calcified *E. huxleyi* cells (B/C or C morphotype). In the subtropical and tropical eastern South Pacific, an exceptionally hyper-calcified R morphotype of *E. huxleyi* (henceforth referred to as R/hyper-calcified; showing the complete fusion of distal shield elements and partial or complete calcite overgrowth of the coccolith central area) was dominant in coastal upwelling waters with relatively high pCO_2/low Ω_{cal} levels, causing an inversion in the trend of calcite-per-coccolith vs. Ω_{cal} seen in the rest of the ocean (Beaufort et al., 2011; von Dassow et al., 2018). Likewise, Smith et al. (2012) observed an increase in the proportion of *E. huxleyi*, corresponding to an "over-calcified" morphotype (with complete overgrowth of the coccolith central area but without fusion of distal shield elements, referred to hereon as A-CC for covered central area) that occurred during the winter

100   decline of Ω_{cal} in the Bay of Biscay (North Atlantic). These results suggested that perhaps the A-CC and R/hyper-calcified morphotypes are likely resistant to low Ω_{cal}. However, while the B/C morphotype was reported to be especially sensitive to low Ω_{cal} compared to moderately calcified and over-calcified strains of morphotype A (Müller et al., 2015), other experimental results did not find a higher resistance of the R/hyper-calcified subtype to high CO_2/low Ω_{cal} when compared to moderate-calcified strains of morphotype A isolated from neighboring waters (von Dassow et al., 2018). These results highlight that it

105   is unclear how the physiological effects of OA on coccolithophores in culturing conditions translate to community-level responses in the field.

    Fjord systems provide especially interesting natural laboratories for observing how coccolithophores may be affected by environmental conditions due to high spatial and seasonal variability in chemical and biotic conditions. In the Norwegian fjord system and the neighboring North Sea, *E. huxleyi* has been very well studied for over a century, where it forms dense spring

110   blooms but is also prominent throughout the year (Birkenes and Braarud, 1952; Berge, 1962; Kristiansen et al., 1994; Fernandez et al., 1996; Egge et al., 2015). Southern Patagonia, on the Pacific side of South America, hosts the largest network of fjords and channels in the world. Aquatic ecosystems of southwest Patagonia (50-55º S) are dominated by the transition between oceanic and estuarine-brackish waters. Denser, saltier, nitrate- and phosphate-rich but silicate-poor Sub-Antarctic Surface Water (SAASW) intrudes below nitrate- and phosphate-poor but silicic acid-rich surface waters influenced by

115   substantial freshwater inputs (copious precipitation, rivers, glacier melt; Dávila et al., 2002; Sievers and Silva, 2008; Torres et al., 2014). Generally, surface waters with low salinity and low alkalinity are undersaturated in dissolved CO_2 during spring-summer seasons (Torres et al., 2011). The Archipelago Madre de Dios (AMD) is an interesting exception to this pattern, where extreme precipitation/runoff in the "limestone" basin on the western AMD produces surface waters with low salinity and high alkalinity while maintaining low dissolved silicate compared with the eastern basin (Torres et al., 2020). These gradients create

120   a unique contrast for exploring the influence of chemical conditions on the ecology of calcified phytoplankton, as changes in Ω_{cal} are driven mainly by freshening rather than upwelling of high pCO_2.

    In contrast to the Norwegian fjord system, *E. huxleyi* blooms have not been reported in Patagonian fjords, however information on coccolithophores in these waters is scarce. A study documenting coccolithophores in the Strait of Magellan found that this group represented a minor fraction of the small-sized phytoplankton (Zingone et al., 2011), but other published studies have

125   not specifically sampled for coccolithophores. The Patagonian shelf on the Atlantic side experiences large *E. huxleyi* blooms (Poulton et al., 2011; 2013), but satellite observations suggest coccolithophore blooms are of lower intensity in the Pacific waters to the west (Hopkins et al., 2019). These observations raise the question of how coccolithophore communities on the western coast and fjords-channels of Patagonia compare with nearby oceans and to fjord systems in the northern hemisphere. Here, we evaluated how physical, chemical, and biological features influence the distribution, abundance, and biomass of

130   coccolithophores as well as the proportions of *E. huxleyi* morphotypes of varying calcification levels throughout southern Patagonia fjords. In particular, three research questions were addressed: i) What coccolithophore assemblages and *E. huxleyi* morphotypes are present in fjords/channels of southern Patagonia? ii) How do these morphotypes and the co-occurring phytoplankton (mostly diatoms) vary with physical and chemical factors? and, iii) Does the abundance and relative

composition of *E. huxleyi* morphotypes reflect populations in adjacent Pacific, Atlantic, or Southern Ocean waters or instead exhibit similarities to the Norwegian fjord system?

2 Materials and methods

2.1 Sampling

Two cruises were conducted onboard the vessel M/N Forrest during the late austral spring 2015 (26 November to 03 December) and early austral spring 2017 (22 to 28 September) in southern Chilean Patagonia ($\sim$ 50-54º S; 71-76º W). The sampling track of 2015 was from the Archipelago Madre de Dios (AMD), crossing the Inner Channel (IC) to the western part of the Strait of Magellan (WSM), and entering eastward into the Otway and Skyring Sounds (OS, SS) to end up near Punta Arenas (Fig. 1a). The 2017 sampling was from the interior WSM, crossing the IC, and ending in the AMD zone (Fig. 1b). In both cruises, surface water (< 5 m) was pumped continuously onboard every 15-20 min for determination of salinity and temperature with a YSI-30 Termosalinometer (Yellow Springs, OH, USA) and pCO_2 with a Qubit-S157 CO_2-analyzer (Kingston, Ontario, Canada). The CO_2-analyzer was calibrated daily with 0 ppm CO_2 (air treated with soda lime) and 403 ppm air-CO_2 mixture standard (Indura, Chile). Surface samples for determination of the planktonic assemblages and chemical variables (i.e., concentration of macronutrients, opal, total chlorophyll-*a*, and the carbonate system parameters) were collected at discrete samplings stations (Fig. 1a-b). Twenty-one stations were sampled in 2015: five in the AMD (St. 1-5), four in the IC (St. 6-9), nine in the WSM (St. 10-12, 16-21), two in the OS (St. 13 and 14), and one in the SS (St. 15). Eleven stations were sampled in 2017: three in the AMD (St. 30-32), five in the IC (St. 25-29), and three in the WSM (St. 22-24).

CTD vertical profiles were additionally obtained at selected localities on both cruises. In 2015, three casts were performed into the AMD zone and one cast into the SS using a CTD Seabird 19 plus (Sea-Bird Scientific, Bellevue, WA, USA) equipped with photosynthetically available radiation (PAR) and oxygen sensors. Two profiles were performed in 2017 in the AMD zone, by the deployment of a CTD Seabird 25 plus with PAR and oxygen sensors. The depth of 1% of penetration of PAR (euphotic zone) was calculated from maximum surface PAR values. CTD profile binning was 1 m. In both years, samples for the determination of plankton assemblages and chemical variables were obtained at discrete depths using 5-L Niskin bottles to which the CTDs were attached (depths pre-determined from prior studies in the region, aiming to adequately sample the surface mixed layer, pycnocline, and vertical variation in chlorophyll fluorescence). Complete environmental and biological data are provided in supplementary materials (Tables S1-S4).

2.2 Plankton assemblages

Samples for the determination of planktonic organisms through the Utermöhl (1958) method were collected only in 2015. For that, duplicate 100-mL water samples were pre-filtered through 200-µm Nitex mesh, fixed with a formaldehyde-glutaraldehyde solution (1% formaldehyde, 0.05% glutaraldehyde, 10 mM borate pH 8.5) and stored at 4º C. In the laboratory, water samples were brought to room temperature, gently homogenized and sedimented into 100-mL chambers for 24-48 h before counting

165 and identification. The absolute abundances of the microplankton (20-200 μm in size) and coccolithophores (~6 μm in diameter) were estimated with an inverted microscope (Olympus CKX41) connected to a digital camera (Motic 5.0). For counts of diatoms, dinoflagellates, and other planktonic cells greater than about 40 μm, the whole chamber was examined at 200× magnification. When large chain-forming diatoms were in high density, between 5-60 randomly selected fields of view were examined at 200× magnification until reaching 100 chains. For counts of small diatoms, naked flagellates (including

170 small flagellates and athecated dinoflagellates), and coccolithophores, between 1-4 transects (to reach ≥ 100 cells in total) were analyzed at 400× magnification. Counts of total coccolithophores were performed with a 40× objective with cross-polarized light (Edmund Optics polarizers 54926 and 53347).
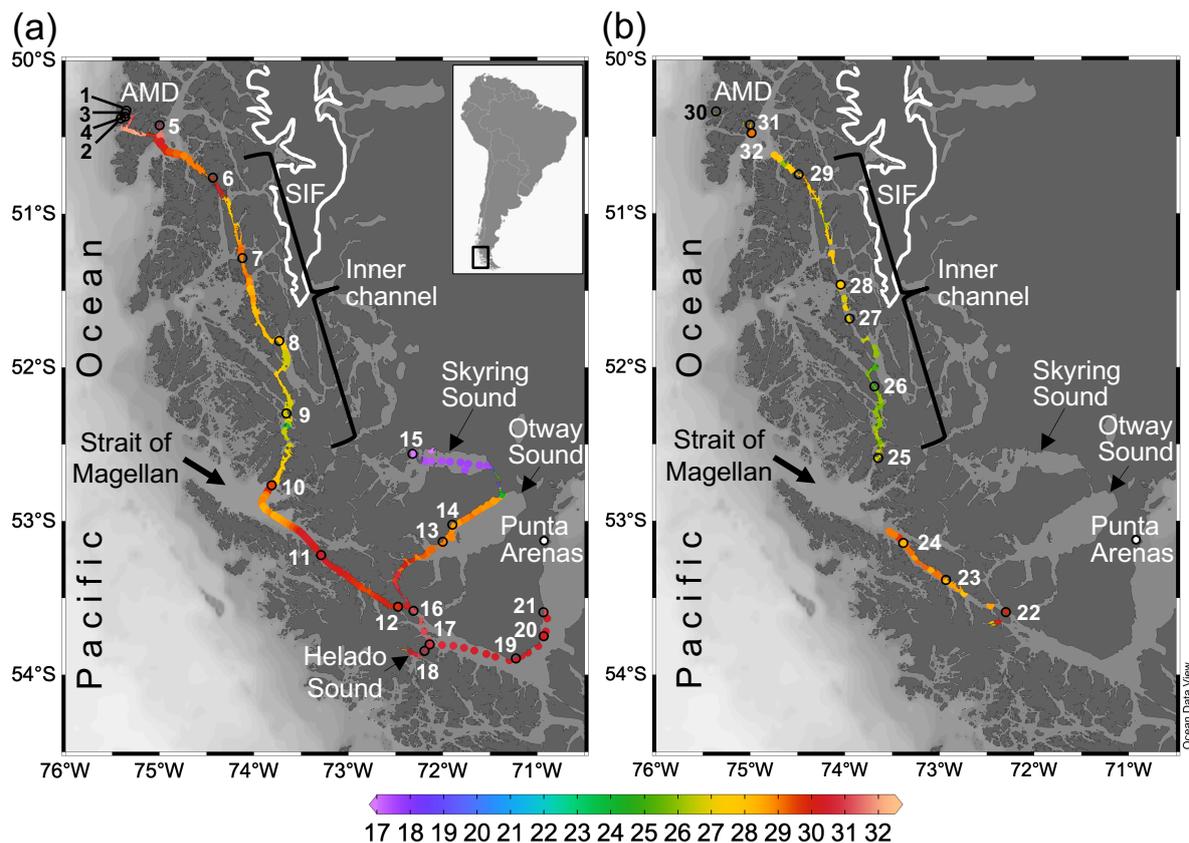

Figure 1. Maps of southern Patagonia showing the study sites and stations sampled during the austral late-spring 2015 (a) and early-spring 2017 (b). Salinity recorded at the surface during the two cruises is plotted. The approximate perimeter of the Southern Ice Fields (SIF) is depicted. A zoom into the Archipelago Madre de Dios (AMD) zone with salinity and Ω calcite surface values recorded in 2015 is provided in supplementary figure S1. Maps produced by Ocean Data View (Schlitzer, 2018).

In both cruises, samples for the identification and quantification of coccolithophores through scanning electron microscopy (SEM) analysis were obtained by filtering 200-300 mL of surface water, immediately after sampling, onto 0.8-μm

175 polycarbonate filters that were subsequently dried at room temperature. For the identification of coccolithophores and *E.*

huxleyi morphotypes, a portion of each dried filter was cut, sputter-coated with gold and examined either in a Quanta FEI 250 or Quanta FEG 250 SEM (both FEI, Hillsboro, Oregon, USA). As water samples for light microscopy counts were not available for two samples from 2015 (St. 3 and St. 5 at 8 m) and all samples from 2017, total coccolithophores abundances were obtained from SEM counts for those samples. On average, 70 images per filter were captured at 1,500× magnification (276×184 μm per frame), covering 3.5 mm^2 of the filter area corresponding to 1.8-3.4 ml of water analyzed. The coccolithophores abundances were calculated using the following equation:

$$cells\ L^{-1}\ = \frac{effective\ filtration\ area\ (mm^2) \times total\ number\ of\ counted\ cells}{analized\ filtered\ area\ (mm^2) \times volumen\ of\ filtered\ water\ (L)}$$

To check for differences in coccolithophore counts obtained through sedimentation + inverted light-microscopy versus filtration + SEM examination (hereinafter SEM and Utermöhl counts, respectively), polycarbonate filters from three selected Utermöhl samples (showing higher, medium and lower coccolithophores abundances) were analyzed with SEM as outlined above. Coccolithophores SEM counts were consistently about twice as high compared to Utermöhl counts (average 1.84), agreeing with the correction factor suggested by Bollmann et al. (2002). Thus, all total coccolithophore counts obtained by the Utermöhl method were multiplied by 1.84 to be comparable to SEM counts. To estimate the absolute abundances at species- and morphotype-level, the relative abundance of each coccolithophore species or *E. huxleyi* morphotype determined from SEM counts was multiplied by the absolute abundance of total coccolithophore cells. Saturation curves obtained for each sample confirmed that the number of analyzed coccospheres (minimum 40 coccospheres per sample) was enough to capture the specific/morphotype diversity.

SEM images taken at 20,000-25,000× magnification were used to categorize *E. huxleyi* cells in the different morphotypes according to the morphology of distal shield and the central plate of the coccoliths (following Young and Westbroek, 1991; Young et al., 2003; Hagino et al., 2011; von Dassow et al., 2018). Given high morphological similarities in the A morphotype coccoliths with those found by Young (1994) in Norwegian-fjords, they were here classified as lightly-, moderate-, and robust-calcified, based on the morphology of distal shields and central plates (Fig. 2; Table 1). Moreover, two extremely heavily-calcified A-morphotypes were observed: the A-CC (with closed central area but distal shield elements mostly not fused) and the R/hyper-calcified (Table 1; Fig. 2). These two morphotypes are sometimes grouped as "over-calcified" (Cubillos et al., 2007; Saavedra-Pellitero et al., 2019). However, we have observed in culture that they remain distinct under different physiological stresses (e.g., Mella-Flores et al., 2018; von Dassow et al., 2018). This analysis assumes discontinuous traits that can be accurately assessed by qualitative analysis. A morphometric study supports this, where coccoliths of what we term the A-CC morphotype cluster well apart from other A morphotype coccoliths in the parameter relative tube length (that is, a small second mode in histograms) (Young et al., 2014). This assumption was also necessary as morphometric analyses in these characters are difficult to measure consistently in field samples and on attached coccoliths. Similarly, due to frequent overlap in coccolith distal shield lengths and coccosphere diameters observed in moderate- and robust-calcified A-forms (Table 1), we consolidate them into one group (hereafter jointly referred to as "moderate-calcified A-morphotype") for statistical analyses. Moreover, we classified the malformed (teratological), incomplete, weakly-dissolved and collapsed coccoliths, following the

terminology and definitions of Young and Westbroek (1991) and Young (1994). Although these malformed and collapsed coccoliths were observed in < 9% of the morphotype-A cells, it was almost always possible to classify those abnormal

210 coccospheres into one of the above-mentioned morphotypes (Fig. S2). SEM images were also used to measure the orthogonal coccosphere diameters and, when available, coccolith distal shield length (ImageJ software version 1.48 for Mac OS).

Biovolumes (μm^3) of *E. huxleyi*, diatoms, dinoflagellates, and naked flagellates were estimated assuming recommended geometric shapes (Hillebrand et al., 1999; see Table S4). For *E. huxleyi*, a spherical geometric shape was assumed and the maximum diameter used for biovolume calculations. Biovolume calculations were then converted to carbon biomass by using

215 regression equations proposed by Menden-Deuer and Lessard (2000) for diatoms (pg C cell^{-1} = 0.288 × volume$^{0.811}$) and other protists (pg C cell^{-1} = 0.216 × volume$^{0.939}$). We assumed a constant cytoplasm diameter to be 60% of the mean *E. huxleyi* coccosphere diameter (O'Brien et al., 2013), whereas cytoplasm volumes of 50% and 78% were used for diatoms and dinoflagellates, respectively (i.e., total cellular volume minus frustule or theca and vacuole volumes; Sicko-Goad et al., 1984). Absolute abundance data were standardized to cells L^{-1} and multiplied by specific carbon contents per cell (pg cell^{-1}) to derive

220 total carbon biomass (Total C; μg C L^{-1}). We used the biogenic silica concentration (μmol opal L^{-1}) as a proxy of diatom biomass along the 2017 track, as samples for microscopy counts were not available. For this, the bSi concentration was converted into carbon units using the average net silicate to carbon ratio of 0.52 (mol/mol) found by Brzezinski et al. (2003) in the Southern Ocean. There was a significant linear relationship between diatom carbon biomass estimated with microscopy/
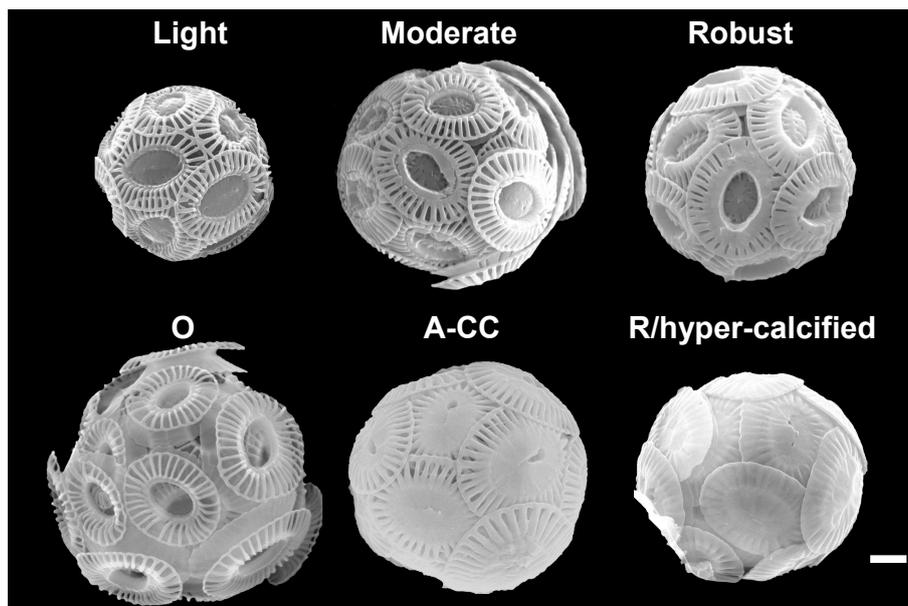

Figure 2. The main *E. huxleyi* morphotypes recorded in the surface waters of southern Patagonia fjords during the austral late-spring 2015 and early-spring 2017. The light-, moderate- and robust-calcified A-morphotypes (top), and the O, A-CC and R/hyper-calcified forms (bottom) are shown. For statistical analysis, the moderate- and robust-calcified A-morphotypes were merged under "moderate-calcified A-morphotype", and the few O and C specimens were categorized into the lightly-calcified subgroup. Scale bar = 1 μm.

Table 1. Classification of *E. huxleyi* coccospheres based on the calcification level of coccoliths. Mean ± standard deviations of distal shield length and coccosphere diameter of morphotypes observed in Patagonia are given for coccospheres where at least one distal shield was visible and adequately oriented (numbers in parenthesis).

Morph	Calcification	Distal shield and central area distinguish features	Distal shield length (µm)	Coccosphere size (µm)	Comparable morphotype	Reference
A	Light	Delicate and well separated distal shield elements (> 50 % of distal shield elements is slits), which end up into a wide central area consisted of plate or lath-like elements	3.3 ± 0.3 (15)	5.7 ± 0.5 (15)	Under-calcified	Young, 1994
A	Moderate	Straight low-profile distal shield formed by thicker elements (< 50-25 % of distal shield area is open between elements) fused to tube elements delimiting a grilled cleanly to semi-open central area	3.5 ± 0.3 (430)	6.3 ± 0.9 (430)	Typical A-morphotype	Young and Westbroek, 1991 Young et al., 2003 Hagino et al., 2011
A	Robust	Robust calcification of elements (< 25 % of distal shield area is open between elements) from partially to nearly completely fused extending from the outer rim to a wide to narrow central area delimited by robust tubes	3.3 ± 0.3 (259)	5.9 ± 0.7 (259)	A over-calcified Type A A calcified	Young, 1994 Henderiks et al., 2012 Saavedra-Pellitero et al., 2019[a]
A	CC	Thicker to robust but not fused elements and central area completely or nearly completely covered	3.0 ± 0.2 (26)	5.7 ± 0.6 (26)	Over-calcified	Young et al., 2003 Cubillos et al., 2007 Smith et al., 2012 Saavedra-Pellitero et al., 2019[a]
A	R/hyper	Heavily calcified distal shield elements completely fused and central area grilled but partly or completely covered	3.7 ± 0.4 (13)	7.2 ± 1.0 (13)	Over-calcified R-type R over-calcified	Cubillos et al., 2007 Beaufort et al., 2011 von Dassow et al., 2018 Saavedra-Pellitero et al., 2019[a]
C and O[b]	Light	Distal shield elements in low-profile and greater coccosphere size compared with light A-morphotype	3.4 ± 0.2 (7)	6.9 ± 1.4 (8)	Type B, Type B/C, Type C	Young and Westbroek, 1991 Young et al., 2003 Hagino et al., 2011

[a] The Plate Ib-c of Saavedra-Pellitero et al. (2019) are grouped together as "over-calcified" in that reference but are distinguished in the present study as R/hyper-calcified and A-CC morphotypes. Plate Ie of Saavedra-Pellitero et al. (2019) corresponds to over-calcified A morphotype in Young (1994) and the present study. Similarly, the "Type A overcalcified" in Fig. 3c of Cubillos et al. (2007) corresponds to the A-CC morphotype here (as distal shield elements are not fused or only partly fused in most coccoliths) while Fig. 3d of the same reference, identified also as "Type A overcalcified" appears to show both nearly complete fusion of distal shield element as well as nearly complete over-calcification covering the central area, so corresponds to the R/hyper-calcified morphotype in the present study.

[b] B and C morphotypes are distinguished by distal shield diameters > 4.5 or < 3.5 µm, respectively, with B/C being intermediate. O variants have varied distal shield diameters with an empty (open) central area (Hagino et al., 2011). B and B/C were not observed in Patagonia. The lightly calcified *E. huxleyi* in the dataset of von Dassow et al. 2018 included a continuum of characteristics from A to B and B/C or C.

allometry and those calculated from bSi concentration in 2015 samples ($R^2 = 0.60$, $p < 0.05$, slope = 0.8; N = 11), with an offset (16 µg C L^{-1}) likely from other contributors to bSi (e.g., silicoflagellates, radiolarians) as well as the contribution of *Minidiscus* spp. (data not shown) not included in microscopy/allometric carbon estimation. The presence/absence of diatoms

was confirmed qualitatively in 2017 by SEM images at 1,500× magnification, and a semi-quantitative evaluation was made as follows: low (few valves), intermediate (at least one species with several valves or chains) and high (many species with several cells or chains). It should be kept in mind that there can be substantial variation in diatom carbon-biomass estimated by microscopy vs. bSi, due to variability in diatom C:Si ratios (Leblanc et al., 2018).

2.3 Chemical analyses

Macronutrients, opal, total chlorophyll-*a* (chlo-*a*), pH and total alkalinity (A_T) were determined as described in Torres et al. (2020). Full carbonate system parameters (including Ω_{cal}) were estimated from pH, A_T, salinity, temperature (25 °C as input and *in situ* temperature as output conditions), pressure (0 dbar as input and depth as output conditions) using CO2Sys Excel macro spreadsheet version 2.1 (Pierrot et al., 2006) with Mehrbach set of solubility constants (Mehrbach et al., 1973) refitted by Dickson and Millero (Dickson and Millero, 1987). To extrapolate full carbonate parameters from pCO_2 (onboard sensor) and salinity measurements where alkalinity samples were not directly available (due to mismatch in chemical and biological sampling along the IC-WSM 2015 track), the regression curve for the salinity-A_T relationship (μmol kg^{-1}) = 63.4 × salinity + 101 (R^2 = 0.99, N = 186; Torres et al., 2020) was used to derive A_T estimated from salinity. It is important to note that this relationship has been stable for over a decade in Patagonia (Torres et al., 2011; Torres et al., 2020). pCO_2 values delivered by the onboard sensor (underway sampling) correlated with pCO_2 calculated from A_T-pH pairs (discrete sampling) in the same 2015 samples (R^2 = 0.56, $p < 0.001$; N = 17), with an overestimation of 6 μatm (2%). The differences between measured and calculated pCO_2 values are small compared to the high ranges in the variability of pCO_2, salinity, A_T, and pH, and should not affect the objectives of the present study. Exceptionally, the calculated pCO_2 values for SS were overestimated by up to 36% concerning pCO_2 measurements (comparing 15 readings from the sensor with three calculated values). This disagreement could be due to various local factors that increase the sensitivity of calculated pCO_2 to A_T (Abril et al., 2015) or pH uncertainties due to differences in salinity between buffers and samples. Therefore, it should be kept in mind that in the case of SS, the uncertainties in the carbonate system could be more substantial. Finally, in order to calculate the bicarbonate (HCO_3^-) to proton (H^+) ratio (in mol/μmol), the HCO_3^- was divided by the antilog$_{10}$ of –pH (total H^+ scale).

2.4 Statistical analysis

All statistical analyses were performed in R software using packages freely available on the CRAN repository (R Core Team, 2019). As measurements for nitrate, phosphate, DSi, bSi, and chlo-*a* in 2015 were scattered and uncoupled from plankton sampling, these variables were used only descriptively and not included in the statistical analyses.

2.4.1 Environmental gradients

Physical-chemical data obtained from the surface at the discrete sample stations both in 2015 and 2017 were combined in a unique matrix and standardized by subtracting the mean and dividing by the standard deviation (Legendre and Legendre, 2012). We used the *varclus* function in the 'Hmisc' package based on Spearman's correlation to detect redundant

environmental variables (N = 32). Temperature, salinity, pH, and Ω_{cal} were selected as they are non-redundant based on Spearman's correlation < 0.75 (Fig. S3) and they are easiest to interpret from a biological or cell physiological point of view. We also included CO_2. It was moderately correlated with pH (Spearman correlation = 0.8), but represents the substrate for photosynthesis and is typically incorporated as a driving variable in ocean acidification studies. HCO_3^- may more directly impact sensitivity of coccolithophores in lab measurements (e.g., Kottmeier et al., 2016; Gafar et al. 2018) but it was redundant with the other variables. The selected standardized variables were then used in two separate cluster analyses to recognize groups of sampling stations with similar characteristics in 2015 (N = 21) and 2017 (N = 11). For that, Euclidean distance matrixes were first calculated based on selected standardized variables (*vegdist* function in the 'vegan' package) and then included in hierarchical cluster analyses based on the Ward method using the *hclust* function in the basic 'stats' package.

2.4.2 Testing for a relationship of *Emiliania huxleyi* vs. diatoms

To characterize the diatom species associated with the different *E. huxleyi* morphotypes and other coccolithophore species, we performed a non-metric multidimensional scaling (nMDS) using the *metaMDS* function in the 'vegan' package, based on the log-transformed [ln (*x*+1)] coccolithophore and diatom abundances (cells L^{-1}) in Patagonia (only 2015) and the other coastal and oceanic locations (von Dassow et al., 2018) (N = 52). The function heatmap of the basic 'stats' package was then used to plot the abundance of the coccolithophore and diatom species related to the clusters based on the nMDS scores of species/morphotypes and samples. As both the nMDS and OMI (see below) analyses suggested a clear separation between Patagonia fjords and the other coastal/oceanic areas, we used the IndVal analysis (Dufrene and Legendre, 1997) to identify indicator species for both areas, based on log-transformed abundances (*indval* function in 'labdsv' package).

We aimed to assess how *E. huxleyi* and diatom biomasses were related to each other and with the environmental conditions throughout Patagonia fjords. However, the different methods used to estimate diatom biomass in both years precluded the use of *E. huxleyi*:diatom ratios. Moreover, the use of regression-based analyses was not recommended due to the absence of a linear relationship between *E. huxleyi* and the different physical-chemical variables. To overcome these limitations, we created three categorical variables for both *E. huxleyi* and diatom biomasses (low, intermediate, and high) based on their < 25, 25-75 and > 75 percentiles, respectively. We then performed a correspondence analysis (CA) using the function *cca* in the 'vegan' package, based on the presence or absence of these new categoric variables in each sample (N = 32), followed by fitting the standardize physical-chemical variables to the CA plot using the *envfit* function (10,000 permutations).

2.4.3 Niche analysis

We used the outlying mean index (OMI) analysis (Dolédec et al., 2000) to assess how the different physical-chemical variables (selected in section 2.4.1) were associated with the realized niche of the different *E. huxleyi* morphotypes. The OMI index represents the marginality (i.e., niche position) and measures the distance between the average habitat conditions used by a given population and the average environmental conditions across the study area (represented by the point where the two multivariate axes intersect at zero). The tolerance (Tol) accounts for the dispersion of samples containing organisms of the

population from the average environmental condition (i.e., niche breadth), whereas the residual tolerance (RTol) accounts for the proportion of the variability unexplained by the variables included in the analysis (Dolédec et al., 2000). Thereby, a species having a low OMI (species score close to zero, located in the center of the multivariate space) and high Tol is likely one that utilizes a wider array of resources and maintains populations within a wider variety of conditions (i.e., generalist), when compared with the specialized and less resilient species with more restricted realized-niche associated to high OMI and low Tol that are expected to show lower Tol and may also be associated with lower OMI (Dolédec et al., 2000).

The OMI analysis was performed using the *niche* function in the 'ade4' package (Dray and Dufour, 2007), considering simultaneously the data obtained for 2015 and 2017 (N = 32). To compare the patterns observed in Patagonia to other localities in the south eastern Pacific, a complementary OMI analysis was performed, including records of coccolithophore assemblages and *E. huxleyi* morphotypes from nearby coastal and oceanic waters (published by von Dassow et al., 2018) in addition to the data used in the first analysis (N = 64). A 1.84× correction factor (determined as informed in section 2.2) was applied to these data, as coccolithophore counts from von Dassow et al. (2018) were obtained by the Utermöhl method. In both cases, data were arranged in two matrices, one containing the coccolithophore abundances and a second matrix with the standardized physical-chemical variables. Coccolithophore abundances were previously Hellinger-transformed (Legendre and Legendre, 2012). Since Hellinger transformation is obtained by the squared root of relative abundances, the potential biases from comparing data from both SEM and Utermöhl counts were minimized. The statistical significance of the morphotypes/species marginality was tested using the Monte Carlo method included in the 'ade4' package (10,000 permutations). The *envfit* function in the 'vegan' package (Oksanen et al., 2007) was then used to fit the five environmental variables to the OMI scores (10,000 permutations).

3 Results

3.1 The late-spring southern Patagonia 2015

The hierarchical clustering based on the surface values of the selected physical-chemical variables in the austral late-spring 2015 (i.e., salinity, temperature, Ω_{cal}, pH and pCO_2) showed a clear separation between the sampling station at the Skyring Sound (SS; st. 15) and the other localities (Fig. 3a). The other stations were grouped in two main clusters: one cluster composed of stations in the Archipelago Madre de Dios (AMD) and the Inner Channel (IC) and a second one composed mainly of stations in the western part of the Strait of Magellan (WSM). Samples from the Otway Sound (OS; sts. 13-14) were distributed between the two clusters. The cluster separation seemed to be mainly related to temperature and salinity dissimilarities, while stations 4 and 15 differed from others by their relatively low pCO_2/high Ω_{cal} and high pCO_2/low Ω_{cal} conditions, respectively (Fig. 3b). Surface salinity ranged from > 29 in the AMD and southernmost WSM stations to as low as 17 in the SS (st. 15), with intermediate values throughout the IC and in the OS (range: 26-29; Fig. 3a-b). A north-south gradient of decreasing surface temperature was recorded from 9.0-10.0 °C around the AMD zone to 7.1 °C near Helado Sound (sts. 17-18; Fig. 3a-b, S4a). Surface waters were mostly undersaturated relative to atmospheric pCO_2 (< 400 µatm) with minimum values at st. 4 in the

12

AMD (241 µatm). CO_2 oversaturation was only observed at the SS (542 µatm). Similar to salinity, Ω_{cal} varied widely, ranging from highly over-saturated conditions in the AMD zone (Ω_{cal} range: 2.5-3.6, pH in situ range: 8.03-8.21), intermediate levels in the interior WSM (Ω_{cal} range: 2.4-2.6; pH range: 8.04-8.07), lower levels in the southern IC zone (Ω_{cal} 2.0-2.2, pH ~8.0) and a sub-saturated extreme reached in the SS sampled site (Ω_{cal} 0.5, pH 7.73, Fig. 3a-b, S5a). Moderate to low DSi (< 6 µM) and nitrate (NO_3^- < 6 µM) were recorded in southern Patagonia, dropping to a minimum in the southern IC zone (Table 2, Fig. S6).
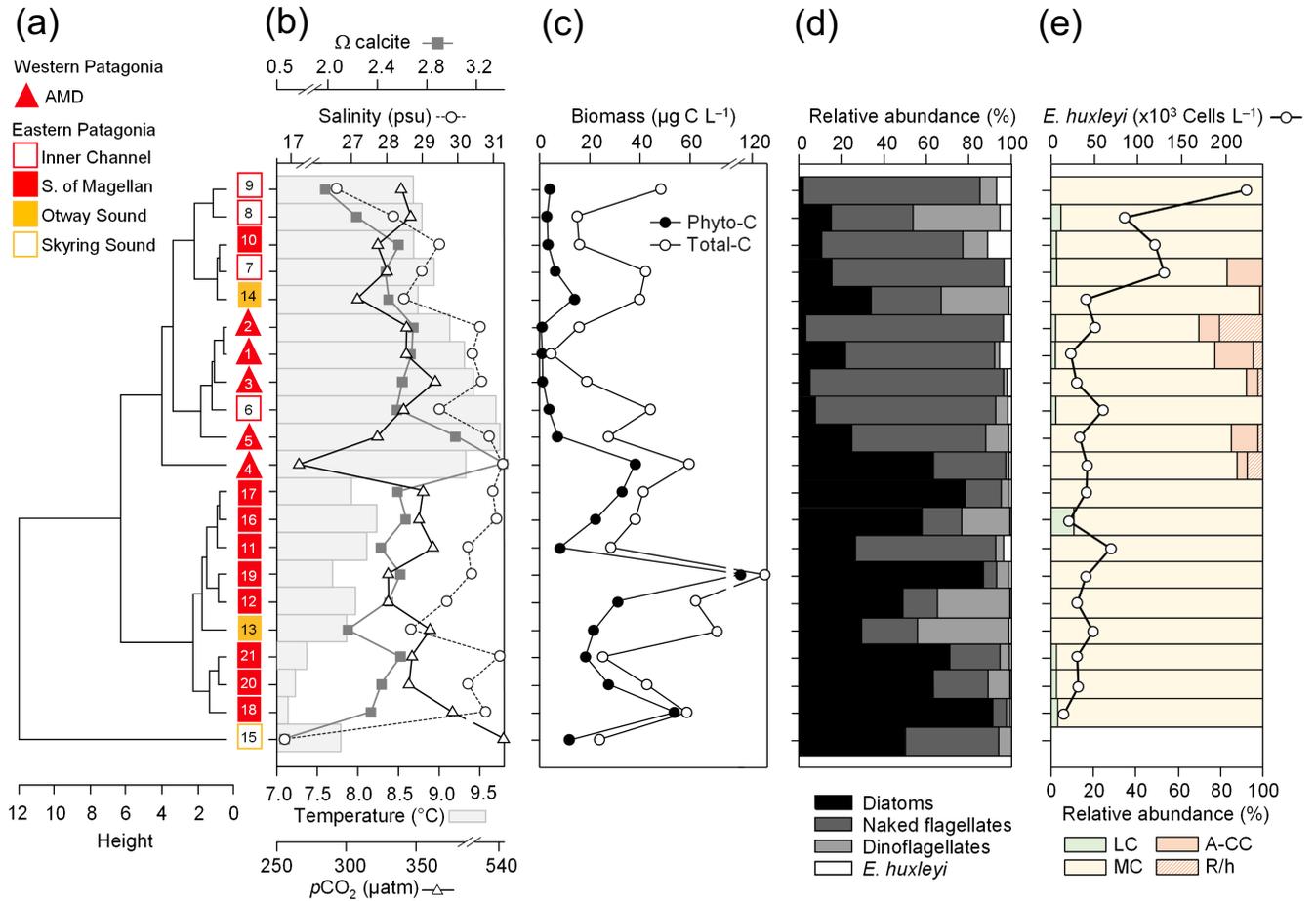

Figure 3. Physical and chemical conditions, carbon biomass by microplankton and phytoplankton assemblages, and abundance and calcification-level of *E. huxleyi* recorded in surface waters of southern Patagonia during the austral late-spring 2015. (a) hierarchical clustering on salinity, temperature, pH, pCO₂ and Ω calcite surface values on 21 water samples collected for plankton analysis, (b) salinity, temperature, Ω calcite, and pCO₂ levels, (c) total carbon biomass by the nano- and micro-plankton assemblages (Total-C, all items between 5-200 µm in length) and phytoplankton assemblages (Phyto-C, diatoms + coccolithophores), (d) relative carbon biomass by diatoms, naked flagellates, dinoflagellates, and *E. huxleyi*, and (e) total abundances of *E. huxleyi* and relative abundances of four *E. huxleyi* morphotypes. All samples were taken < 5 m in depth. Stations 5-7, 11-13, 18-21 were conducted at night. LC = *E. huxleyi* lightly-calcified A-morphotype, MC = *E. huxleyi* moderate-calcified A-morphotype, A-CC = *E. huxleyi* A-CC morphotype, R/h = *E. huxleyi* R/hyper-calcified morphotype.

330   The AMD and IC zones showed relatively low phytoplankton biomasses (< 20 µg C L^{-1}) dominated by naked flagellates (Fig. 3c-d), whereas diatoms were associated with higher phytoplankton biomasses (> 40 µg C L^{-1}) in Eleuterio Channel (st. 4; mostly chains of *Chaetoceros* spp.) and the WSM (sts. 12, 16-21; mostly chains of *Leptocylindrus* spp., *Chaetoceros* spp., and *Thalassiosira* spp.). The contribution of dinoflagellates to biomass was highest in IC st. 8, OS sts. 13-14 and WSM sts. 12 and 16. Coccolithophores only accounted for 0.2-12.8% of total-C biomass (0.1-4.0 µg C L^{-1}), reaching $> 6\%$ only in the southern

335   IC (sts. 8-10) where diatom biomasses were among the lowest observed. *E. huxleyi* dominated the coccolithophore assemblages in all samples ($> 98\%$), with a few *Syracosphaera* spp. coccospheres (mostly collapsed) found at the AMD (Table S2). *E. huxleyi* abundances (Fig. 3e) ranged from 0 to 2.76×10^5 cells L^{-1}, being most abundant in southern IC ($> 1.03 \times 10^5$ cells L^{-1} in sts. 7-10) and only absent from SS (st. 15), which was the only station where conditions were undersaturated with respect to calcite ($\Omega_{cal} < 1$). *Emiliania huxleyi* populations were mostly composed of the moderate A morphotype (which also included

340   cells of the robust-calcified A-morphotype; see Methods) (Fig. 3e, Table 3). Few lightly-calcified A cells were observed. Among all samples, only eight total O and C and no B or B/C morphotype cells were detected. The heavily A-CC and R/hyper-calcified morphotypes were restricted to the AMD zone.

Table 2. Physical and chemical conditions, and photosynthetic and silicified biomass proxies in the surface waters (< 5 m) of southern Patagonia fjords. Mean, standard deviation (SD) and range of each variable and number of samples for the late-spring 2015 and early-spring 2017 are shown. Only values matching planktonic samples discussed in the text are included, except for chlorophyll-*a* (Chlo-*a*), opal, nitrate and silicate 2015 for which values are between 3-28 km decoupled from biological sampling. The mean and SD do not include the Skyring Sound 2015 station as it shows extreme values for all variables (see Table S1). However, the values from that sample are shown in parenthesis for comparison. n.a = no available data.

Survey	Late-spring 2015			Early-spring 2017		
	Mean ± SD	Range	*n*	Mean ± SD	Range	*n*
Temperature (ºC)	8.6 ± 0.9	(7.8) 7.1 – 10.0	22	7.1 ± 0.6	6.3 – 8.1	12
Salinity	30.0 ± 1.2	(16.9) 26.6 – 31.3	22	27.9 ± 1.3	25.1 – 29.8	12
pCO$_2$ (µatm)	337 ± 33	241 – 386 (542)	22	368 ± 28	320 – 412	12
Ω calcite	2.6 ± 0.4	(0.5) 2.0 – 3.6	22	2.0 ± 0.3	1.5 – 2.4	12
CO$_3^{2-}$ (µmol kg^{-1})	106 ± 15	(21) 79 – 150	22	83 ± 11	59 – 96	12
HCO$_3^-$ (µmol kg^{-1})	1,739 ± 61	(1,144) 1,572 – 1,811	22	1,701 ± 60	1,606 – 1,811	12
pH (total scale)	8.07 ± 0.04	(7.73) 8.03 – 8.21	22	8.02 ± 0.03	7.95 – 8.08	12
A_T (µmol kg^{-1})	2,006 ± 80	(1,197) 1,773 – 2,097	22	1,911 ± 79	1,757 – 2,037	12
DIC (µmol kg^{-1})	1,861 ± 67	(1,193) 1,667 – 1,935	22	1,802 ± 66	1,687 – 1,920	12
HCO$_3^-$/H$^+$ (mol/µmol)	0.205 ± 0.023	(0.061) 0.168 – 0.274	22	0.179 ± 0.016	0.144 – 0.203	12
Chlo-*a* total (µg L^{-1})	2.0 ± 1.1	(0.49) 0.3 – 5.4	24	1.9 ± 1.3	0.2 – 3.9	12
Opal (µmol L^{-1})[a]	0.8 ± 0.4	0.5 – 1.8 (2.1)	13	1.7 ± 0.7	0.6 – 2.8	12
Nitrate (µmol L^{-1})	3.3 ± 1.3	(0.32) 0.5 – 6.1	24	9.0 ± 2.0	6.0 – 12.8	12
Silicate (µmol L^{-1})[a]	2.3 ± 1.8	(1.5) 0.2 – 6.1	13	5.3 ± 3.1	2.2 – 12.4	12
Phosphate (µmol L^{-1})	n.a.	n.a.	--	0.7 ± 0.2	0.3 – 1.0	12

[a] 2015 range is from the Archipelago Madre de Dios to the inner channel zone along 50.4-52.6º S.

Table 3. Relative percentages of *E. huxleyi* A-morphotypes recorded throughout southern Patagonia fjords. Mean, standard deviation (SD), and maximum and minimum percentages of five *E. huxleyi* morphotypes recorded in inner surface waters of southern Patagonia (PAT; *n* = 883 cells counted in 23 samples) and down to 50 m in the Archipelago Madre de Dios western zone (AMD; *n* = 1,012 cells counted in 27 samples) during the austral late-spring 2015 and early-spring 2017.

Morphotype/ Sample set	Lightly-calcified			Moderate-calcified			Robust-calcified			A-CC			R/hyper-calcified		
	Mean ± SD	Max.	Min.	Mean ± SD	Max.	Min.	Mean ± SD	Max.	Min.	Mean ± SD	Max	Min.	Mean ± SD	Max.	Min.
PAT 2015+2017	2.6 ± 3.1	10.8	0	62.7 ± 18.7	97.5	26.3	34.5 ± 18.9	71.1	2.5	0.1 ± 0.5	2.5	0	0	---	---
AMD 2015+2017	3.4 ± 7.1	33.3	0	40.4 ± 14.6	65.8	8.3	39.0 ± 14.8	72.5	15.0	12.4 ± 9.5	41.7	2.5	4.8 ± 5.4	20.5	0

345 Three vertical profiles were performed in the AMD estuarine zone (Fig. 4): one at the "limestone" western AMD basin (st. 3), one between the western and eastern AMD basins (st. 4), and one at the easternmost basin (st. 5, Fig. 4, S1). All samples were taken within the euphotic zone (1% PAR), which extended down to 36 and 30 m in sts. 3 and 4, respectively (st. 5 was conducted at night, Fig. S7a-c). All three sites were sharply stratified in the upper 10 m, with pycnoclines around 5 m. Temperature decreased while salinity increased with depth (Fig. 4a-c). In station 3, Ω_{cal} varied little with depth, remaining in

350 the range 2.5-2.7 (Fig. S7g) even across the shallow pycnocline. In station 4, Ω_{cal} showed the highest values and highest range; A_T, pCO2, and HCO3$^-$ increased sharply with depth in the upper 10 m, while Ω_{cal} decreased from over 3.6 to less than 2.9 at 9 m, and 2.7 at 29 m (Fig. S7h). Finally, at station 5, Ω_{cal} decreased steadily from 3 at the surface to 2.4 at 25 m (Fig. S7i). Based on total chlo-*a* levels and fluorescence signals, most photosynthetic biomass occurred in the upper 15 m of the water column in sts. 3-4, peaking at the surface in st. 4 (5.4 µg L^{-1}). However, in station 5, total chlo-*a* levels and fluorescence signals were

355 more constant with depth, dropping proportionally less by 25 m from maximal values, when compared to the other stations. The "Silicate" estuarine zone (st. 4-5) showed higher photosynthetic biomass and bSi than the "limestone" site (Fig. 4a-c, S7d-f). *Emiliania huxleyi* mostly occurred in the well-illuminated upper layer, most notably in the "limestone" western AMD waters, where diatom abundance and biomass were low compared to the communities recorded in "silicate" sites (Fig. 4d-f). Although the moderate A morphotype was predominant at all depths in the three stations (Fig. 4g-i), a higher proportion of the A-CC

360 morphotype (up to 31% relative abundance) was observed in the upper 15 m of the "limestone" western AMD when compared to the other two stations. The lightly-calcified and R/hyper-calcified morphotypes were present in a lower proportion (<10%).
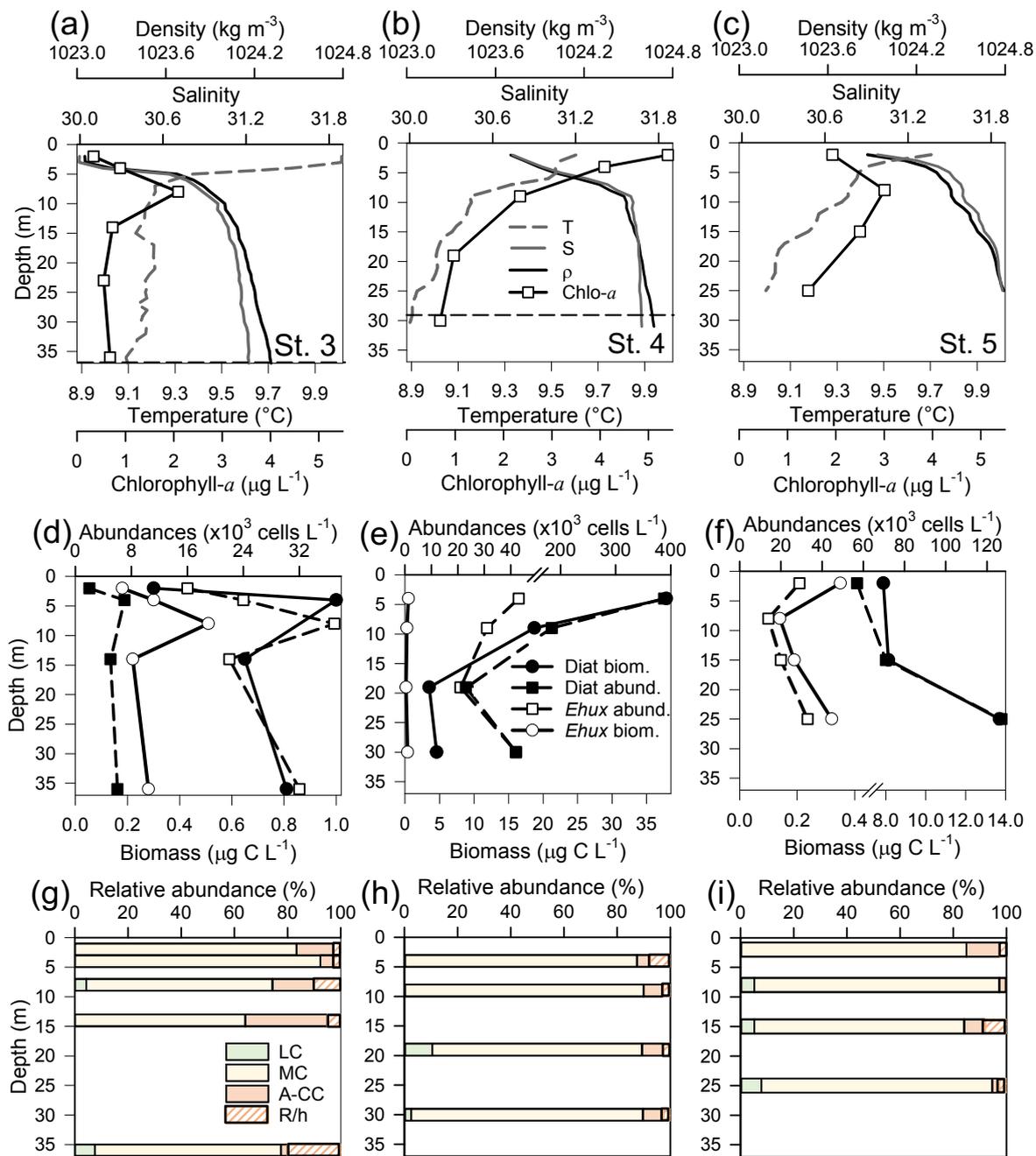
Figure 4. Physical, chemical, and biological vertical profiles recorded in the Archipelago Madre de Dios during austral late-spring 2015. Temperature, salinity, density and total chlorophyll-*a* (a-c), abundance and total carbon biomass of *E. huxleyi* (*Ehux*) and diatoms (Diat; d-f), and relative abundance of four *E. huxleyi* morphotypes (g-i) in the W-AMD (st. 3 left), between (st. 4 middle), and E-AMD zones (st. 5 right). Dotted lines in panels a-b indicate depths of 1% PAR penetration (st. 5 was conducted at night). Morphotype abbreviations as in Fig. 3. See Fig. S7 for additional variables.

3.2 The early-spring southern Patagonia 2017

The hierarchical clustering based on the physical-chemical conditions in austral early-spring 2017 indicated a separation between the WSM and the IC, whereas the three stations in the AMD were distributed between the two clusters (Fig. 5a). Surface salinity ranged from 25 to 30 along the south-north track, with saltier waters (> 28) around the AMD (sts. 30-32) and southward in the WSM zone (sts. 22-24), and fresher waters in the southern IC (< 27 at sts. 25-27) (Fig. 5b). Surface temperatures ranged from a minimum of 6.3 °C in the southern IC to > 7.7 °C in the AMD and northern IC (max. 8.1 °C in st. 29, Fig. 5a-b, S4b). Surface waters were undersaturated with respect to pCO_2 in all stations (range: 320-396 µatm) except for station 26 (412 µatm). Lower Ω_{cal} levels prevailed in the southern IC (range: 1.5-1.9) with higher Ω_{cal} in the AMD zone (range: 2.1-2.4; Fig. 5b, S5b). Nitrate, silicate and phosphate concentrations (Fig. 5c) were mostly in the range 6.0-8.3, 2.2-5.4, and 0.3-0.7 µM, respectively, with the highest levels of nitrate (9.5-12.8 µM) and phosphate (0.8-1.0 µM) in sts. 22-23, 26 and 30, whereas stations 30 and 26 registered the highest DSi (12 and 7 µM, Fig. 5c, Table 2). Higher photosynthetic biomass (chlo-a > 2.7 µg L^{-1}) was recorded around the eastern AMD (st. 29, 31-32) and WSM station 23, while the western AMD (st. 30), southern IC (st. 25-26), and WSM (st. 22) yielded the lowest measured biomass (chlo-a < 1.3 µg L^{-1}; Fig. 5d). Variation in chlo-a reflected variation in diatom biomass (Fig. 5d).

The dominant coccolithophore taxon during early-spring 2017 was again *E. huxleyi* (> 96%). Abundances ranged from 1.69×10^4 to 9.06×10^4 cells L^{-1} (Fig. 5e). The *E. huxleyi* carbon biomass averaged 0.5 ± 0.3 µg C L^{-1} (in 11 samples), reaching both maximal and minimal values (0.2 and 1 µg C L^{-1}, respectively) in the southern IC (sts. 25-27). In contrast, the opal-derived diatom carbon biomass averaged 40 ± 17 µg C L^{-1}, with lower values (< 18 µg C L^{-1}) in the AMD st. 30 and IC st. 25 (Fig. 5d). While fixed samples for standard microplankton analysis were not available, large chains of *Skeletonema* spp., *Thalassiosira* spp., and *Chaetoceros* spp. were noted as frequent in samples observed by SEM (Fig. S8), and were likely significant contributors to opal. Similar to the 2015 survey, the moderate A morphotype dominated the *E. huxleyi* assemblages along the 2017 track (Fig. 5e). Cells of the lightly-calcified A morphotype were sporadically observed, whereas the highly-calcified A-CC and R/hyper-calcified morphotypes were again restricted to the AMD zone (Fig. 6, Table S1; note the low abundances of the R/hyper-calcified morphotype were only detected at other depths, so do not appear in Fig. 5e).

Two CTD profiles were performed in the AMD zone: one in the "limestone" western AMD basin (st. 30) and another profile southwest of Escribano Island at the "silicate" eastern AMD basin (st. 32) (Fig. 6a,b). The profiles covered the euphotic zone (down to 27 m in st. 32; st. 30 was conducted at night) as well as sub-surface layers (25-75 m depth). In both stations, temperature and salinity increased with depth, with maximum density stratification between 5-10 m. In the western AMD profile, Ω_{cal} was low at the surface (2.1) due to the lowest salinity, but rose to a maximum at 5 m due to a minimum in pCO_2 and increasing salinity, whereas below 20 m, pCO_2 rose and Ω_{cal} dropped (Fig. S9e). At the eastern AMD site, in contrast, Ω_{cal} increased with depth despite increasing pCO_2 (Fig. S9f). At both stations, photosynthetic biomass was mainly confined to the upper 25 m of the water column, with chlo-a peaks at 5 and 10 m (0.7 and 3.1 µg L^{-1}, respectively), and dropping close to zero below 40 m in the western AMD, while remaining near 1 µg L^{-1} even at depths ≥50 m in the eastern AMD (Fig. 6a-b, S9a-b).

The eastern AMD zone exhibited higher chlo-*a* and bSi when compared to the western AMD, despite no depletion of phosphate, nitrate and DSi were observed at either site (Fig. 6a-b, S9a-d).

At both sites, *E. huxleyi* dominated the coccolithophore assemblages across all depths, with another six coccolithophore species observed in sub-surface AMD waters (Table S3). *E. huxleyi* and diatom abundances were highest in the surface at both sites (Fig. 6c-d). However, reflecting the chlo-*a* profile, estimated diatom biomass remained relatively high at depth compared to surface values (dropping by only about 40%), and *E. huxleyi* abundance and biomass also dropped less with depth in the eastern AMD compared to the western AMD (Fig. 6c-d). In both stations, the composition of *E. huxleyi* morphotypes was similar at all depths, characterized by the predominance of the moderately-calcified morphotype followed by highly-calcified A-CC (Fig. 6e-f). The lightly-calcified and R/hyper-calcified morphotypes were either undetected or represented a minor fraction of coccolithophore assemblages.
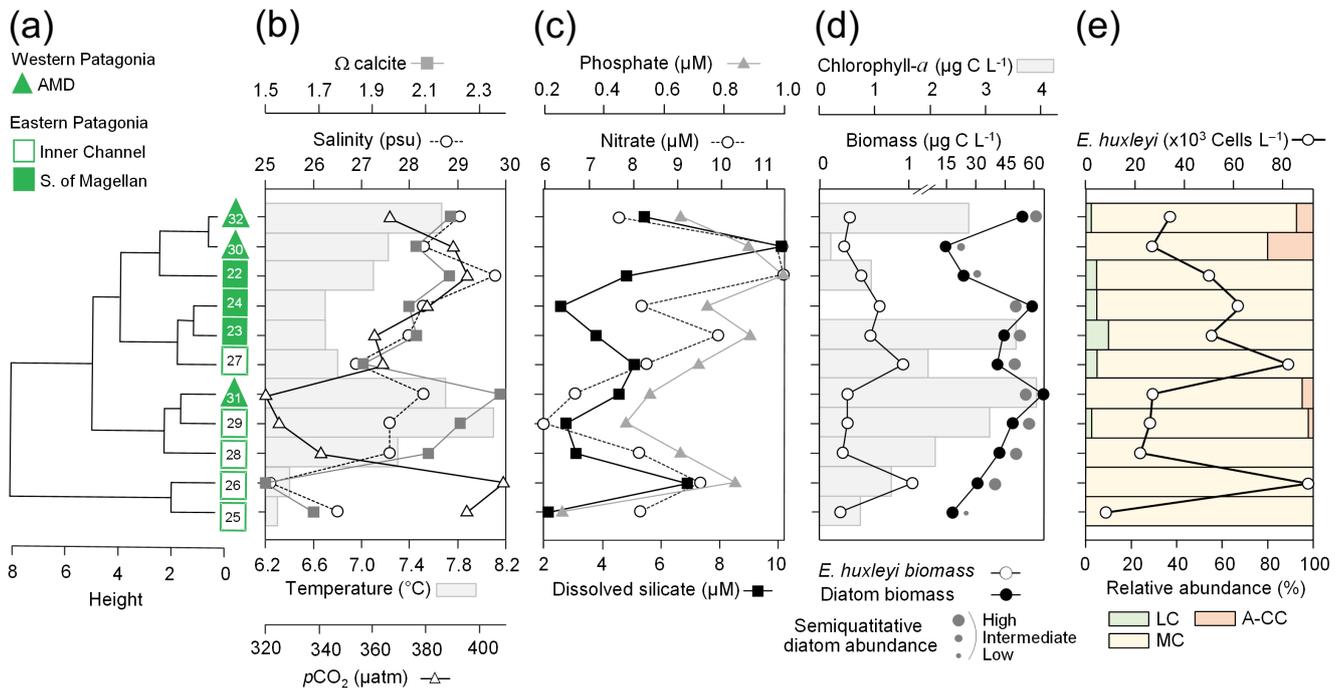

Figure 5. Physical, chemical and nutrient conditions, chlorophyll-a levels, carbon biomass by *E. huxleyi* and diatoms, and abundances and calcification-level of *E. huxleyi* recorded in surface waters of southern Patagonia during the austral early-spring 2017. (a) hierarchical clustering on temperature, salinity, pH, pCO2 and Ω calcite surface values on 11 water samples collected for plankton analysis, (b) salinity, temperature, Ω calcite and pCO2 levels, (c) nitrate, dissolved silicate, and phosphate levels, (d) total chlorophyll-a and total carbon biomass by *E. huxleyi* and diatoms, and semi-quantitative estimation of diatom abundances (SEM), and (e) total abundances of *E. huxleyi* and relative abundances of three *E. huxleyi* morphotypes. All samples were taken < 5 m in depth. Stations 25-26 and 30 were conducted at night. Morphotype abbreviations as in Fig. 3.
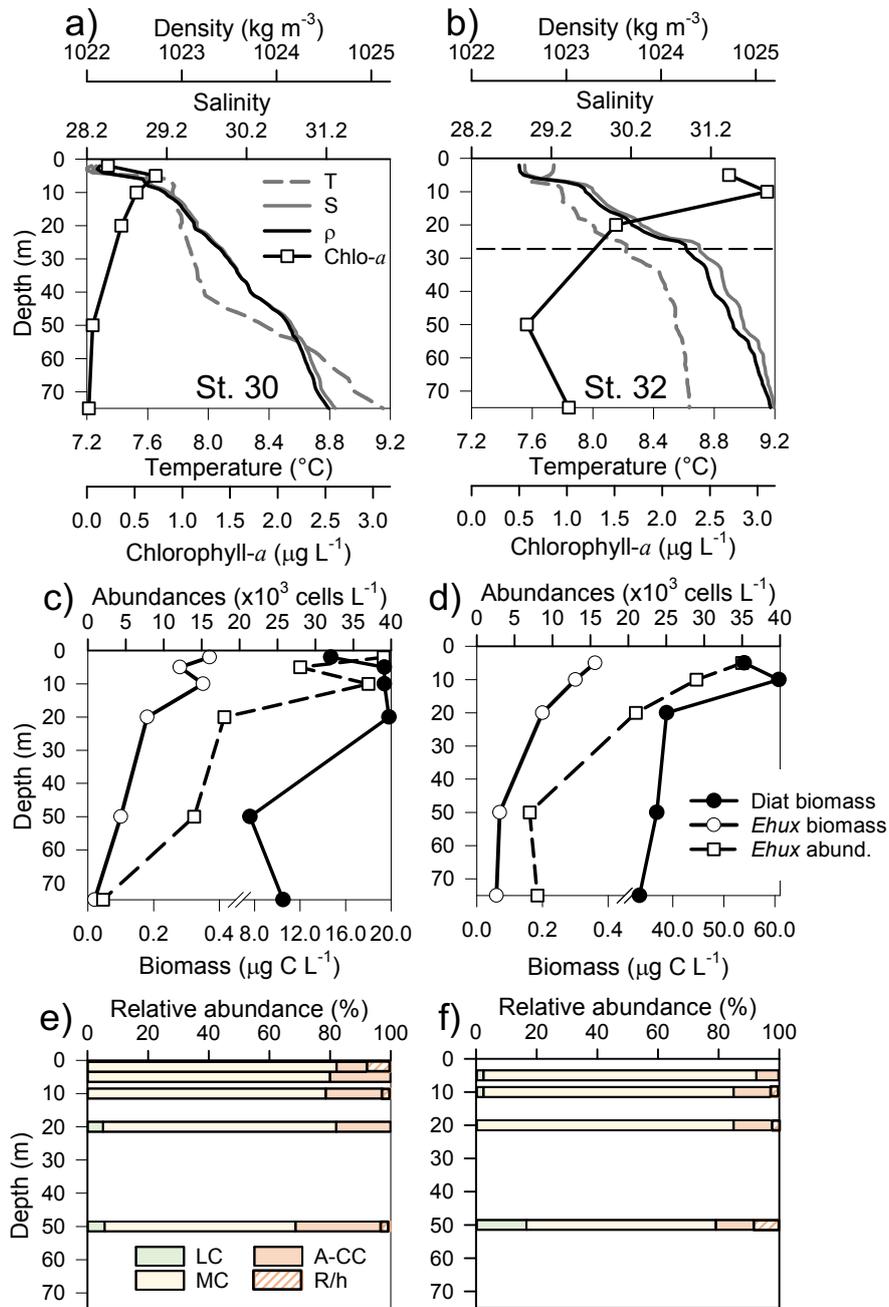
Figure 6. Physical, chemical, and biological vertical profiles recorded in the Archipelago Madre de Dios during the austral early-spring 2017. Temperature, salinity, density, and total chlorophyll-*a* (a-b), abundance of *E. huxleyi* and total carbon biomass of *E. huxleyi* (*Ehux*) and diatoms (Diat; c-d), and relative abundances of four *E. huxleyi* morphotypes (e-f) in the W-AMD (st. 30 left) and the E-AMD (st. 32 right). Dotted line in panel b indicates depth of 1% PAR penetration (st. 30 was conducted at night). Morphotype abbreviations as in Fig. 3. See Fig. S9 for additional variables.

3.3 *Emiliania huxleyi* abundance vs. diatoms

The nMDS depicted a clear separation between the Patagonia fjords and the oceanic/coastal areas regarding the composition of coccolithophorid and diatom assemblages (Fig. 7). The IndVal analysis (Table S5) identified only the *E. huxleyi* moderate-calcified morphotype as an indicator of the fjord locations, along with the diatoms *Thalassiosira* spp., *Stephanopyxis turris*, *Leptocylindrus* spp. and *Chaetoceros* spp. The coastal/oceanic locations were more characterized by the lighty-calcified and A-CC morphotypes and the other coccolithopore species (i.e., *G. ericsonii, G. muellerae, G. parvula*), as well as the diatoms cf. *Lioloma* spp., Pennate diatoms (< 50 μm length), *Nitzschia* spp., cf. *Pseudo-nitzschia cuspidata*, and cf. *Asteromphalus sarcophagus*.

The two first axes of the CA accounted for 60% of the total explained variability and indicated that the highest *E. huxleyi* and low diatom biomasses were associated with increasing temperatures (Fig. 8). Intermediate *E. huxleyi* biomasses were associated with high diatom biomasses and increasing gradients of salinity, pH and Ω_{cal}, whereas low *E. huxleyi* biomasses were associated with intermediate diatom biomasses and increasing pCO_2. However, none of the considered environmental variables had a significant fit in the *envfit* test.
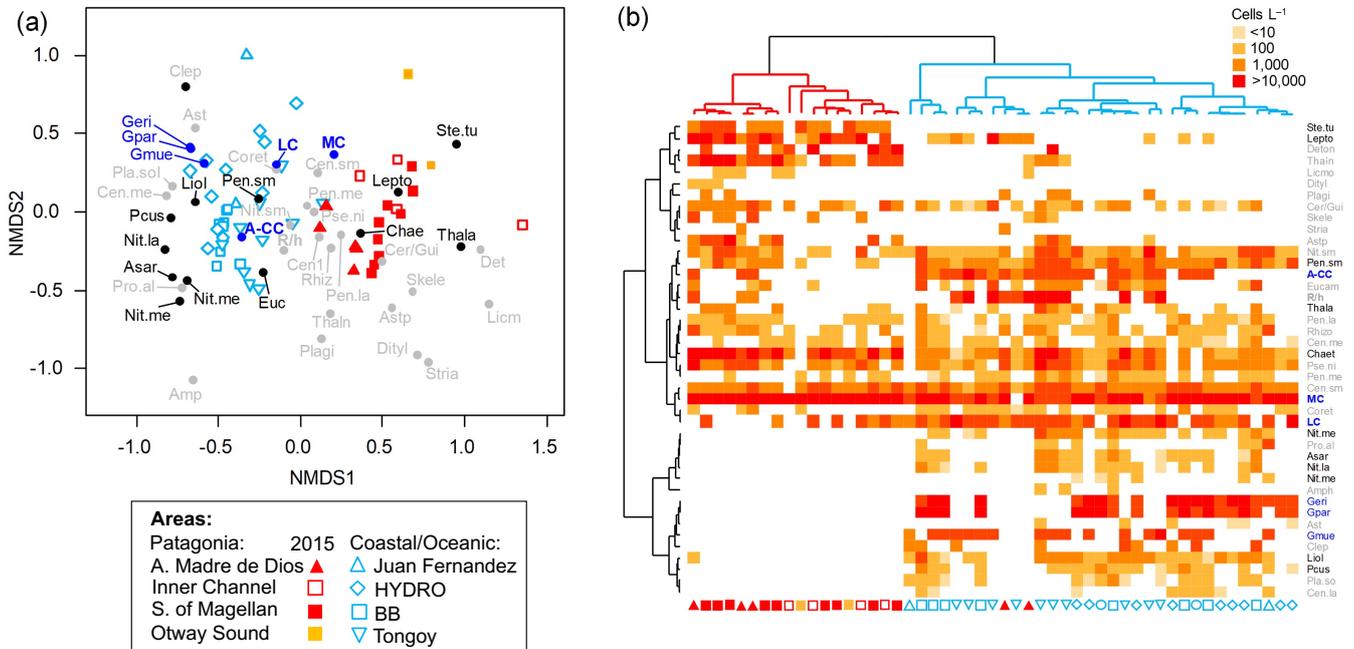
Figure 7. (a) Non-metric multidimensional scaling (nMDS) based on coccolithophore and diatom abundances attained in southern Patagonia fjords during late-spring 2015 (this study) and other coastal/oceanic areas (data from von Dassow et al., 2018). (b) Heatmap showing abundances of coccolithophore and diatom species used in the nMDS. The horizontal dendrogram (based on the nMDS samples scores) shows a clear separation between Patagonia fjords (red cluster) and coastal/oceanic (blue cluster) areas, whereas the vertical dendrogram (based on the nMDS species scores) indicates the separation of species in two main clusters. Black and blue species labels depict species with significant values in the IndVal analysis. A-CC = *Emiliania huxleyi* A-CC morphotype; Amphi = *Amphiprora* spp.; Asar = cf. *Asteromphalus sarcophagus*; Aster = *Asteromphalus* spp.; Astp = *Asterionellopsis* spp.; Cen.la = Centric diatoms > 100 μm diameter; Cen.me = Centric diatoms 40-100 μm diameter; Cen.sm = Centric diatoms < 40 μm diameter;

Chae = *Chaetoceros* spp.; Clep = *Calcidiscus leptoporus*; Coret = *Corethron* spp.; Cer/Gui = *Cerataulina* spp. + *Guinardia* spp.; Deton = *Detonula* spp.; Dityl = *Ditylum* spp.; Eucam = *Eucampia* spp.; Geri = *Gephyrocapsa ericsonii*; Gmue = *Gephyrocapsa muellerae*; Gpar = *Gephyrocapsa parvula*; LC = *Emiliania huxleyi* lightly-calcified morphotype; Lepto = *Leptocylindrus* spp.; Licmo = *Licmophora* spp.; Liol = cf. *Lioloma* spp.; MC = *Emiliania huxleyi* moderate-calcifield morphotype; Nit.la = *Nitzschia* spp. large > 100 um length; Nit.me = *Nitzschia* spp. medium 100-50 um length; Nit.re = *Nitzschia reversa*; Nit.sm = *Nitzschia* spp. < 50 μm length; Pcus = cf. *Pseudo-nitzschia cuspidata*; Pen.la = Pennate diatoms > 100 μm length; Pen.me = Pennate diatoms 50-100 μm length; Pen.sm = Pennate diatoms < 50 μm length; Pla.so = *Planktoniella sol*; Plagi = *Plagiogrammopsis* spp.; Pro.al = *Proboscia alata*; Pse.ni = *Pseudo-nitzschia* spp.; R/h = *Emiliania huxleyi* R/hyper-calcified morphotype; Rhizo = *Rhizosolenia* spp.; Skele = *Skeletonema* spp.; Ste.tu = *Stephanopyxis turris*; Stria = *Striatella* spp.; Thala = *Thalassiosira* spp.; Thaln = *Thalassionema* spp.
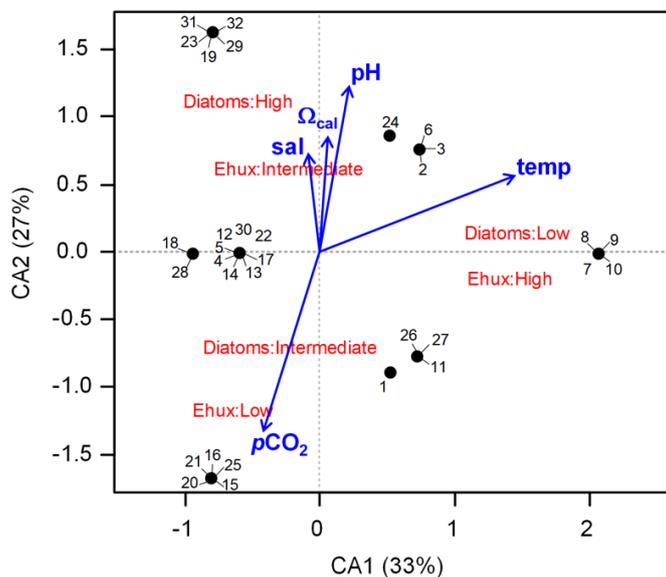

Figure 8. Correspondence analysis (CA) assessing the relationship between *E. huxleyi* and diatom biomasses converted to categoric values (i.e., low, intermediate, and high biomasses) in Patagonia fjords during late-spring 2015 and early-spring 2017. The *envit* function of the 'vegan' package (R software) was used to fit the environmental variables to the CA plot (no variable was significant; $p > 0.05$).

3.4 Niche analysis of *Emiliania huxleyi* morphotype responses to environmental conditions

The OMI analysis depicted differences in the realized niches of the *E. huxleyi* morphotypes throughout Patagonian fjords in 2015 and 2017 (Fig. 9a, Table S6). The OMI plot showed station 15 from 2015 as an outlier, characterized by extremely low salinity and high pCO_2. The OMI axis 1 (91.02% of explained variability) was negatively related to Ω_{cal}, whereas the OMI axis 2 (8.42 % of explained variability) was positively related to salinity and pH and negatively related to temperature and pCO_2. The *envfit* test indicated that all variables had a significant fit ($R^2 > 0.88$, $p < 0.01$; Table S7). Only the moderate A and R/hyper-calcified morphotypes showed significant OMIs ($p < 0.05$, Table S6). The moderate A morphotype was the most generalist (OMI = 0.07, Tol = 1.23), observed in all samples (except st. 15 in 2015). The R/hyper-calcified morphotype, observed exclusively in the AMD zone, was the most specialized morphotype (OMI = 4.77, Tol = 0.75). The A-CC morphotype (OMI = 1.43, Tol = 1.68), observed in the AMD and northern IC, showed intermediate habitat preferences (Fig. 9a), but the OMI for this morphotype did not meet the threshold for significance ($p = 0.060$). The RTol for the R/hyper-calcified

morphotype was 12% (Table S6), indicating that most variability in its realized niche was accounted for by the environmental variables included in the analysis.

The extended domain OMI analysis (Fig. 9b, Table S8) indicated a clear separation between the Patagonian fjords and coastal and oceanic waters off central and northern Chile and Peru. The OMI axis 1 (74.57% of explained variability) was negatively related to temperature, salinity and Ω_{cal}, whereas the OMI axis 2 (25.32 % of explained variability) was positively related to pH and negatively related to pCO_2. The *envfit* test indicated that all variables had a significant fit ($R^2 > 0.88$, $p < 0.01$; Table S9). All coccolithophore species and *E. huxleyi* morphotypes showed significant OMIs ($p < 0.05$, Table S8). The lightly-calcified, moderate-calcified and A-CC morphotypes, characterized as the most generalists, showed similar realized niches (OMI = 0.25-0.75, Tol = 2.85-2.96), whereas the R/hyper-calcified form was again the most specific of the *E. huxleyi*
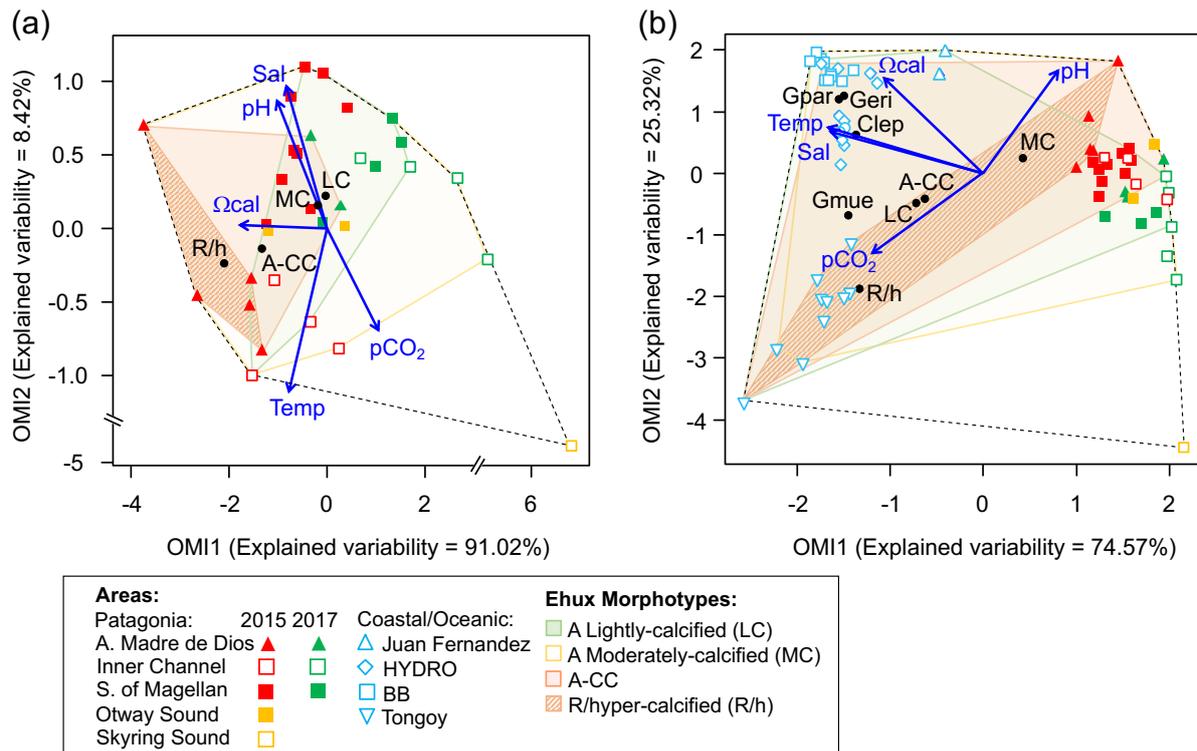

Figure 9. Outlying Mean Index (OMI) niche analysis by *E. huxleyi* (*Ehux*) morphotypes populating the surface waters of southern Patagonia, and complemented with coccolithophores and *Ehux* morphotypes from nearby coastal and oceanic waters constrained by environmental conditions. (a) Biplot representing the realized-niche of four *E. huxleyi* morphotypes during the austral late-spring 2015 and early-spring 2017 in Patagonia, where black circles indicate the mean habitat condition used by each morphotype (niche-position) and polygons delimit their respective niche-breadth (i.e., tolerance). Blue vectors represent the gradients of environmental variables. (b) Realized-niches of *Ehux* morphotypes and other coccolithophore species in Patagonia fjords (this study) and nearby coastal/oceanic waters (data from von Dassow et al., 2018). Polygons of other coccolithophore species in (b) are not shown for simplicity. Temp = temperature, Sal = salinity, LC = *E. huxleyi* lightly-calcified A-morphotype, MC = *E. huxleyi* moderate-calcified A-morphotype, A-CC = *E. huxleyi* A-CC morphotype, R/h = *E. huxleyi* R/hyper-calcified morphotype, Gpar = *Gephyrocapsa parvula*, Geri = *Gephyrocapsa ericsonii*, Gmue = *Gephyrocapsa muellerae*, Clep = *Calcidiscus leptoporus*.

morphotypes (OMI = 5.25, Tol = 1.97) and restricted to the coastal upwelling and AMD zones (Fig. 9b, Table S8). Regarding the other coccolithophore species, *G. muellerae* was common to both coastal and oceanic areas but still showed a higher degree of specialization (Tol = 1.03) than the *E. huxleyi* morphotypes, whereas *C. leptoporus*, *G. ericsonii* and *G. parvula* showed preference for oceanic conditions with low Tol values (0.15-0.38; Table S8). The R/hyper-calcified morphotype, *G. ericsonii* and *G. parvula* showed very low RTol (< 4.6%), indicating that most of their realized-niche variation was accounted for by environmental variables in the analysis (Table S8).

4 Discussion

4.1 Patagonian coccolithophore communities dominated by *E. huxleyi*

Emiliania huxleyi was the only coccolithophore widely distributed along the fjords and inner channels of southern Patagonia and always represented > 96% of total coccolithophore abundance and > 89% of coccolithophore biomass, during both early/late spring. The low diversity of coccolithophores assemblages, dominated by *E. huxleyi*, is a common spring-summer feature in both the Patagonian and Norwegian fjord systems. In the case of southern Patagonia, the neighboring Pacific has higher diversity (Beaufort et al., 2008; Menschel et al., 2016; von Dassow et al., 2018), but the Southern Ocean assemblages also show low diversity dominated by *E. huxleyi* (Cubillos et al., 2007; Saavedra-Pellitero et al., 2014; Charalampopoulou et al., 2016; Saavedra-Pellitero et al., 2019). The low diversity in southern Patagonian waters thus may partly reflect this latitudinal trend, although more detailed seasonal studies, including sampling along vertical profiles, might reveal significant additional coccolithophore diversity in the Patagonian and Norwegian fjords.

4.2 Abundance of *E. huxleyi* in Patagonia compared to nearby oceans

During the early/late spring, standing stocks of *E. huxleyi* in the Patagonian fjords and inner seas were moderate compared with those documented in nearby coastal and oceanic regions and within the range of background stocks reported in the Norwegian fjords and North Sea (Table 4 and references therein). The high *E. huxleyi* abundances typical of spring blooms in the Norwegian fjords were not observed in either early or late spring in the present study despite the similar temperature, salinity, and Ω_{cal} conditions in both fjord systems. No *E. huxleyi* blooms have been reported in Patagonia fjords, although this might be due to limited observations and methodological issues. For example, many phytoplankton studies in the area (e.g., Alves-de-Souza et al., 2008; González et al., 2013) as well as standard phytoplankton monitoring in the zone (Vivanco and Seguel, 2009) often rely on samples fixed with acid-Lugol's, which would not preserve coccoliths, or have only focused on larger phytoplankton size classes (e.g., Paredes et al., 2014). Shallow water depth and frequent cloud cover limit satellite observations of PIC within the Patagonian shelf and fjords, but moderate coccolithophore blooms (of lower intensity compared to the North Sea) may occur later in the summer in the Pacific sector offshore of the latitudes sampled here (Hopkins et al. 2019).

Table 4. Comparison of *E. huxleyi* standing stocks and morphotypes recorded in northern and Patagonia fjords systems and nearby coastal/ocean locations. Temperature and salinity ranges are shown. Only data < 10 m in depth were included. ESP = Eastern South Pacific, SO = Southern Ocean, APS = Atlantic Patagonian Shelf, SU = summer, SP = spring, WI = winter, AU = autumn, n.a. = no available data.

Location	Concentration cells ×10³ L⁻¹	*E. huxleyi/* Coccolith.[a]	Main Morph	Year/ Season	Temp. range	Salinity range	References
- Northern Hemisphere fjords:							
Oslo fjord	24 – 36,000[b]	n.a.	n.a.	1939/SU	8.2 – 19.6	8.2 – 28.4	Birkenes and Braarud, 1952
Western coast and fjords	250 – 115,000[b]	n.a.	n.a.	1955/SU	11 – 15	28 – 33	Berge, 1962
Oslo fjord	385 – 14,500[b]	n.a.	n.a.	1981/SU	16 – 20	20 – 21	Paasche and Kristiansen, 1982
Bokna fjord	3,000 – 4,000[b]	n.a.	n.a.	1981/SU	11 – 13	28 – 30	Erga, 1989
Samnanger fjord	<10 – 7,000[c]	n.a.	A	1992/SU	8 – 10	10 – 30	Kristiansen et al., 1994; Young, 1994
Fauskangerpollen, Nordåsvannet	1 – 28,000[b]	n.a.	n.a.	1993/SP	7 – 16	15 – 30	Fernández et al., 1996
- Nearby coastal and oceanic zones:							
Norwegian Sea	200 – 3,000[d]	dominant	n.a.	1987 – 1992	6 – 10	> 35	Samtleben et al., 1995
Norwegian Sea	<10 – 3,000[d]	dominant	n.a.	1987 – 1995	6 – 10	> 35	Baumann et al., 2000
Outer Oslo fjord, Skagerrak	All year round[e]	n.a.	n.a.	2009 – 2011	2 – 16	22 – 33	Egge et al., 2015
Outer Oslo fjord, Skagerrak	171 – 254[d]	n.a.	A	2013/SU	18.5	23.7	Gran-Stadniczeñko et al., 2017
Northeast Atlantic and North Sea	100 – 1,500[f]	dominant	A, B	1990/SU	n.a.	n.a.	van Bleijswijk et al., 1991
North and Norwegian Seas	<3 – 900[d]	40 – 100	A[i]	2008/SU	11 – 18	30 – 35	Charalampopoulou et al., 2011
- Patagonia fjords:							
W. Magellan Straits ~ 52-54° S	~ 100[b]	dominant	n.a.	1991/SU	n.a.	n.a.	Zingone et al., 2011
Fjords and channels ~ 50-54° S	12 – 276[b]	> 98	A	2015/SP	7.1 – 10.0	26.6 – 31.3	This study
Fjords and channels ~ 50-54° S	17 – 91[d]	> 96	A	2017/SP	6.3 – 8.1	25.1 – 29.8	This study
- Nearby coastal and oceanic zones:							
ESP along ~16-20° S; 73-80° W	1 – 34[g]	8 – 99	A	1964/SU	21.9 – 24.9	n.a.	Hagino and Okada, 2006
ESP along ~30-33° S; 72-98° W	up to 350[h]	60 – 90	A, R[j]	2004/SP	14.8 – 19.8	34.1 – 35.1	Beaufort et al., 2008; 2011
ESP along ~35-38° S; 73-78° W	12 – 134[b]	> 50	A, R[j]	2004/SP	10.7 – 15.3	33.4 – 34.6	Menschel et al., 2016
ESP along ~12° S; 77-78° W	1 – 531[b]	> 76	A, R[j]	2014-15/AU,SP	14 – 21	35 – 35.2	Alvites, 2016
ESP along ~13-33° S; 70-86° W	1 – 76[b]	30 – 100	A, R[j]	2011-13/SP,WI	12.3 – 19.8	33.8 – 35.5	von Dassow et al., 2018
SO Pacific ~ 45-55° S; 80-100° W	n.a.	50 – 100	C	1967-1970	1 – 14	n.a.	McIntyre et al., 1970
SO Pacific ~ 54-58° S; 80-97° W	31 – 61[d]	dominant	C, B/C	2009/SU	4.3 – 5.7	~34.1	Saavedra-Pellitero et al., 2014
SO Drake Passage ~ 57-62° S	1 – 580[d]	> 80	B/C	2009/SU	2 – 10	33.7 – 34.0	Charalampopoulou et al., 2016
SO Drake Passage ~ 56-62° S	1 – 214[d]	dominant	B/C	2016/SU	2 – 10	33.3 – 34.0	Saavedra-Pellitero et al., 2019
APS along ~38-54° S; 51-63° W	180 – 3,060[d]	dominant	B/C	2008/SP	7 – 18	33.4 – 35.6	Poulton et al., 2011; 2013

[a] *E. huxleyi* as a component of larger coccolithophore assemblages. When information about other coccolithophore assemblages was provided, the percentage abundance of *E. huxleyi* is given or if it was noted that *E. huxleyi* was dominant. " n.a" means no information about other coccolithophores was provided. [b] estimated through sedimentation chamber and inverted microscopy, [c] estimated by Palmer-Maloney chamber and inverted microscopy, [d] estimated through filtration and scanning electron microscopy analysis, [e] estimated through high-throughput sequencing and operational taxonomic units (OTUs) analysis they found *E. huxleyi* throughout the year but concentrated between summer-autumn, [f] cultured strains were identified at morphotype-level by use immunofluorescence assay, and abundances estimated through scanning electron microscopy analysis, [g] estimated through filtration and cross-polarized microscope, [h] estimated using an automated coccosphere recognition software, [i] the " characteristic" *E. huxleyi* morphotype showed in Fig. 4, [j] the R/hyper-calcified morphotype dominating the *E. huxleyi* assemblages in neritic zones.

4.3 Variation in *E. huxleyi* with environmental factors

It has been previously proposed that the realized niche of *E. huxleyi* is partly defined by physical and chemical conditions unfavorable to large diatoms (Tyrrell and Merico, 2004; Smith et al. 2017). During late-spring Patagonia fjords, *E. huxleyi* reached higher abundances in the southern IC when the temperature was above 8 °C and macronutrients, and larger diatoms were the lowest, consistent with the pattern previously reported more generally for nano-phytoplankton based on size-fractionated chlo-*a* for this geographic area (e.g., Cuevas et al., 2019). However, the CA analysis showed that the lowest levels of *E. huxleyi* were associated with intermediate levels of larger diatoms, and intermediate levels of *E. huxleyi* were associated with highest levels of larger diatoms, suggesting a unimodal relationship between these two planktonic groups, possibly affected by factors not assessed in this study, such as nutrients supply and mixed layer depth (Margalef, 1978; Cermeño et al., 2011), or predation (Nejstgaard et al., 1997).

The Ω_{cal} – the saturation state of calcite, a parameter often assumed to constraint calcification (e.g., Zondervan et al., 2001; Kleypas et al. 2006; but see Cyronak et al. 2016) – was subject to large spatial variations in surface waters, from relatively high Ω_{cal} levels in the AMD zone (range: 2.1-3.6), moderate Ω_{cal} in the interior WSM, low Ω_{cal} in the southern IC (range: 1.5-2.2) and sub-saturating in the SS (0.5). The range of surface Ω_{cal} recorded along southern Patagonia was comparable to those reported for the Norwegian seas (Jones et al., 2019). Whereas the highest Ω_{cal} values observed at the AMD were not as high as those observed in the global ocean (Takahashi et al., 2014), the lower values at the southern IC were comparable to values reported previously (range: 1.8-2.8) from high CO_2 upwelling conditions in central and northern Chile (Beaufort et al., 2008, 2011; von Dassow et al., 2018). While low surface Ω_{cal} at coastal waters of northern and central Chile are related to the upwelling of high pCO_2-DIC enriched subsurface waters, the freshening (and the associated drop in DIC, salinity, and Ca^{2+} caused by dilution) and latitudinal/seasonal cooling (enhancing CO_2 solubility) have major roles in lowering CO_3^{2-} and Ω_{cal} in southern Patagonia. These contrasting systems offered the possibility to observe if the ecological trends related to low Ω_{cal} depend on context.

4.4 Comparison of *E. huxleyi* morphotypes in Patagonia to nearby oceans and Norwegian fjords

There was some variability in the vertical distribution of the *E. huxleyi* morphotypes in the water column. The lightly-calcified coccoliths appeared associated with subsurface waters in both seasons sampled at the locations, so they might be associated with intrusion of these waters. However, the samples within the euphotic zone were generally similar to each other within a given sample station. Thus, for the purposes of the questions in this study, the use of surface samples to describe morphotype distributions is expected to be reasonable, but use of vertical profiles might have permitted a higher ability to explain variability in the OMI analysis.

The *E. huxleyi* populations in the Patagonian fjords were morphologically distinct from surrounding coastal or open ocean populations in the eastern South Pacific, the Southern Ocean, and the Atlantic. The Atlantic Patagonian Shelf *E. huxleyi* populations are reported to be dominated by B/C morphotypes (Poulton et al., 2011, 2013). Southern open ocean populations

of *E. huxleyi* are dominated by B morphotypes (including the B, B/C, C, and O types; Saavedra-Pellitero et al., 2014; Saavedra-Pellitero et al., 2019), and A morphotypes were reported to represent only a small fraction. However, C and O morphotypes were very rare in Patagonian inland waters, and B and B/C morphotypes were undetected. Although the moderate-calcified and robust-calcified A morphotypes have also been shown to be present in eastern South Pacific coastal and open ocean waters (von Dassow et al., 2018), the dominance of these A morphotypes was particular to Patagonian interior waters. This conclusion was supported by the IndVal analysis (Table S5), where moderate-calcified and robust-calcified A morphotypes were consolidated for final statistical analyses as they are not easily distinguished by objective morphological characters, were present in all samples, and preliminary analysis revealed completely overlapping realized niches. Both the moderate-calcified and robust-calcified A morphotypes are also observed as dominant in the Norwegian fjords (Table 4) (Young, 1994). The lightly-calcified A morphotype was rare, and did not show any clear pattern in its distribution. The A-CC morphotype has been associated with coastal upwelling zones in the Atlantic (Giraudeau et al., 1993; Smith et al., 2012; Henderiks et al., 2012) but not reported from the Norwegian fjords or the Southern Ocean. In both early/late spring, the R/hyper-calcified and A-CC *E. huxleyi* appeared only at the Pacific border of southern Patagonia (AMD zone). Thus, *E. huxleyi* populations of both Patagonian fjords and Norwegian fjords share a similar morphotype composition.

4.5 Niche analysis of *E. huxleyi* morphotypes related to carbonate chemistry conditions

The broader niche-breadth by the moderate-calcified A morphotype contrasted with the marginal niche of the R/hyper-calcified forms in Patagonia (Fig. 9a). The lightly calcified A morphotype also showed a low tolerance (more specialist), but this was not statistically significant. In order to extend the realized-niches derived in Patagonia, we complemented the OMI analysis with a sample set of nearby oceanic and coastal sites (data from von Dassow et al., 2018), in some of which the moderate-calcified A morphotype, unlike in Patagonia, was less abundant than other *E. huxleyi* morphotypes and coccolithophore species. According to OMI analysis, the niche-differentiation along Patagonia is mostly driven by the pH/Ω_{cal} conditions, but temperature and salinity conditions also become important. In this extended domain, both the moderate-calcified A morphotype and the A-CC morphotype appeared to be generalists, with high Tol values (Fig. 9b). The lightly-calcified morphotype also appeared to be a generalist in the extended domain. However, we caution that while the lightly calcified *E. huxleyi* were almost exclusively lightly-calcified A morphotype in Patagonia, there was a continuum of lightly-calcified A, B, and B/C morphotypes (and some lightly calcified cells were difficult to classify among these types) in some of the coastal and oceanic sites. Proper differentiation between B, B/C, and C based on coccolith length would require strict morphometrics, which we did not perform due to the difficulty in accurate measurements on full coccospheres of less common morphotypes, especially in low abundance populations (as coccospheres may lack coccoliths in a correct orientation for accurate measurement). Thus the generalist behavior of lightly-calcified morphotypes in the OMI analysis that combined fjord, coastal, and open ocean sites is likely an artefact. We suspect that lightly calcified A, B, B/C, and C morphotypes might actually each exhibit specialist behaviors in distinct but overlapping niches. In fact, a laboratory study reported that B/C morphotype strains only calcified substantially in a relatively narrow range of carbonate conditions (Müller et al., 2015). In contrast, the very

545   distinct R/hyper-calcified morphotype exhibited restricted preferences in terms of Ω_{cal}, temperature, and salinity, but a broad niche in terms of CO_2 and pH (Fig. 9b).

    The R/hyper-calcified morphotype, in which there is both fusion of distal shield elements and closure or partial closure by over-calcification of the central area, has so far only been reported as prevalent in high CO_2/low pH upwelling zone of the eastern South Pacific (Beaufort et al., 2011; Alvites, 2016; von Dassow et al., 2018), although it has been seen (and reported

550   as rare) in both Australian waters (Cubillos et al., 2007) and the Drake Passage (Saavedra-Pellitero et al., 2019). Experimental findings that the R/hyper-calcified morphotype did not perform better than the moderate-calcified A morphotype under high CO_2/low pH/low Ω_{cal} (von Dassow et al., 2018) might be explained by the OMI analysis suggesting a possible narrow unimodal response to Ω_{cal}, that would not have been detected in the experiments of von Dassow et al. (2018), where Ω_{cal} values of 1.4 vs. 3.3 were tested in the lab. The studies of Langer et al. (2009) and Müller et al. (2015) did find that R morphotype strains

555   did seem more resistant to high CO_2/low pH than other A morphotypes, either in growth rate or in PIC production. Those studies used either four-fold higher light levels (Langer et al., 2009) or continuous light (Müller et al., 2015), and low light has been shown to increase the sensitivity to OA specifically of an R morphotype strain (Rokitta and Rost, 2012), highlighting that the R/hyper-calcified morphotype might be selected by interactions with other variables. Alternatively, the R/hyper-calcified morphotype might be selected by an unidentified condition particular to the Southeastern Pacific that correlates with the Ω_{cal},

560   temperature, and salinity of its realized niche.

    The present study shows that the OMI analysis can be useful for identifying how parameters may determine the realized niches of both species and genetically-determined phenotypic variants within a species. For example, in the extended domain (Fig. 9b), Ω_{cal}, temperature, and salinity were important in defining the narrowness vs breadth of niches among the *E. huxleyi* A morphotype, *E. huxleyi* R/hypercalcified morphotype, and closely related *Gephyrocapsa* species, while the habitat centers

565   (niche positions) of the different *E. huxleyi* morphotypes lined up approximately on a gradient of pH vs CO_2. Calcification rate has been demonstrated to vary among *E. huxleyi* strain according to maximum photosynthetic rate, but also CO_3^{2-} concentration at their sites of origin, while maximum photosynthetic rate also varied among the strains with CO_2 at the site of origin (Rickaby et al., 2016). Several recent studies have called into question the importance of Ω_{cal} in determining the response of calcifying organisms, with both theoretical and laboratory support that the concentrations of HCO_3^-, CO_3^{2-}, and H^+ are more important

570   (Kottmeier et al., 2016; Bach et al., 2015; Gafar et al., 2018). However, while HCO_3^-, CO_3^{2-} were formally excluded from the OMI analyses as redundant variables, these vary more with and CO_2 and pH, respectively, which formed an axis along which the niche of the R/hyper-calcified morphotype was broad, rather than the orthogonal gradient in Ω_{cal}. We caution that calcification rate might not relate in a simple way to the morphotypes observed here. Nevertheless, such trade-offs offer crucial clues into how traits related to calcification may be selected by the environment, resulting in the environmental patterns

575   observed here. It might be worth exploring experimentally if there is a role for Ω_{cal} separate from other carbonate parameters in selecting the R/hypercalcified morphotype.

    The OMI analysis presented here was limited as we focused mostly on the carbonate system, and this may be reflected in that sometimes half of the total variability was not explained by included variables. As mentioned above, several studies have

shown that light can impact sensitivity of *E. huxleyi* to OA (Rokitta and Rost, 2012; Jin et al., 2017), although the effect reported differs in some studies (Zhang et al., 2019). The trade-offs in energy and C balances reported by Rickaby et al. (2016) would suggest that light and mixed-layer depth might also be important parameters to consider in future studies. Nutrient limitation can also modify calcification, although a careful chemostat study suggested that nutrient and CO_2 impacts were independent (Müller et al., 2017). The impact of biotic factors were also not assessed with the OMI analysis here, though it is still not clear whether coccoliths might play roles in defense against either grazing or viruses (Harvey et al., 2015; Strom et al., 2018; Johns et al., 2019; Haunost et al., 2020).

A striking result from the OMI analysis was that all the *E. huxleyi* morphotypes, even the more specialized R/hyper-calcified type, exhibited much greater niche breadth (higher Tol values) than the other coccolithophore species. The three *Gephyrocapsa* species are very close relatives of *E. huxleyi* and phylogenetically should be considered as congenerics (Bendif et al., 2016; Bendif et al., 2019), but all showed lower niche breadth than the *E. huxleyi* morphotypes. The small *G. parvula* and *G. ericsonii* showed Tol values that were more than 10-fold lower than the most specialist *E. huxleyi* morphotype. Despite the evidence for a genetic underpinning of *E. huxleyi* morphotypes (Krueger-Hadfield et al., 2014), as well as evidence of a high level of genomic content variability in *E. huxleyi* (von Dassow et al., 2015), phylogenetic and phylogenomic evidences do not clearly support for it to be split into different species (Bendif et al., 2016; Filatov, 2019). If the ubiquitous taxon is less susceptible to environmental change compared to marginal taxa (i.e., marginality or richness vs. tolerance are inversely correlated; Dolédec et al., 2000; Hernández et al., 2015), the exceptional generalist behavior exhibited by *E. huxleyi* compared to other coccolithophores suggests it may be more plastic and more adaptable in the face of environmental change.

The lower values of pH and Ω_{cal} observed here approached levels predicted for higher latitudes of the global ocean at the end of the century under high emission scenarios such as RCP 8.5 (Feely et al., 2009; Hartin et al., 2016). Our results suggest that ongoing changes in ocean chemistry may result in decreases in coccolithophore diversity, leading to more numerical dominance of *E. huxleyi* compared to other coccolithophores, as well as decreased phenotypic diversity within *E. huxleyi*. The extended-domain niche analysis in the present study would suggest that *C. leptoporus* might be less adaptable than *E. huxleyi*. Some studies found that *C. leptoporus* was relatively resistant to OA in the lab (Langer et al., 2006), but others reported that it is sensitive and that its PIC/POC ratio, considered important in determining ballast effects, is especially negatively affected by OA. Species such as *C. leptoporus* can be much more important than *E. huxleyi* in carbonate export due to their production of much heavier coccolithophores which sink faster and dissolve more slowly (e.g., Ziveri et al., 2007; Menschel et al., 2016; Menschel and González, 2019). Thus, a change to more *E. huxleyi*-dominated coccolithophore communities might negatively impact carbonate export.

5 Conclusions

Our study of how *E. huxleyi* abundances and morphotypes respond to the highly dynamic physical and chemical environments of southern Patagonia yielded seven principal findings:

1. The only coccolithophore that was a regular and ubiquitous component of the phytoplanktonic assemblages throughout the surface waters of the southern Patagonian fjords/channels was *E. huxleyi*. It occurred under a wide range of carbonate chemistry conditions and was only absent in the Skyring Sound zone where $\Omega_{cal} < 1$.

2. Although *E. huxleyi* never reached more than a small fraction of total plankton carbon biomass (< 13 % of nano- and microplankton assemblages counted by microscopy), it reached moderate abundances (range: 12-276 x10^3 cells L^{-1}) comparable to adjacent coastal and oceanic areas, and within the lower range of stocks reported from Norwegian fjords (1-115,000 x10^3 cells L^{-1}).

3. *Emiliania huxleyi* abundance was highest (> 100x10^3 cells L^{-1}) when assemblages of large diatoms were lowest (< 10x10^3 cells L^{-1}), in late-spring waters with lower macronutrients, consistent with it being most important in the absence of large diatoms.

4. 4. In terms of morphotypes, the *E. huxleyi* populations in the southern Patagonian fjords/channels were similar to Norwegian fjords (dominated by moderately-calcified and robust-calcified A morphotype) and very distinct from populations previously documented in the Southern Ocean/Drake Passage, and the Patagonian Shelf of the Atlantic (where C or B/C morphotypes were reported as dominant) and from the Eastern South Pacific coastal upwelling zone, where the R/hypercalcified morphotype dominated.

5. Niche analysis shows that the moderate A morphotype and A-CC morphotypes are generalists, whereas the R/hyper-calcified morphotype has a more marginal (specialized) realized niche.

6. The association of the R/hyper-calcified morphotype to high Ω_{cal} in southern Patagonia, where Ω_{cal} is driven principally by freshwater input, contrasts with its dominance in the upwelling system of central Chile to Peru, where low Ω_{cal} is due to high CO_2. This morphotype occupies a narrow range of Ω_{cal} values compared to the ACC and moderate A-morphotypes.

7. The moderate A, A-CC, and R/hyper-calcified *E. huxleyi* morphotypes all display higher niche breadth (more generalist behavior) than closely related coccolithophores, suggesting that *E. huxleyi* may be ecologically more plastic and have more capacity for adaptation in the face of environmental change than other coccolithophores.

Data availability

Sample availability

Supplement

See supplementary material.

Author contributions

FDR (Conceptualizaton; Investigation; Data curation; Formal Analysis; Writing – original draft preparation; Writing – review
& editing) lead the study, carried out sampling in 2015 survey, carried out light and SEM microscopic analysis, conducted
characterization of microplankton and *E. huxleyi* assemblages and morphotype composition, performed biovolume/allometric
analysis, analyzed the relationships between *E. huxleyi* and environmental and biological variables, and wrote the first drafts
of paper. PvD (Conceptualizaton; Funding acquisition; Supervision; Validation; Visualization; Writing – original draft
preparation; Writing – review & editing) trained and supervised FDR in *E. huxleyi* assemblages quantification and
characterization, guided analysis strategies performed extensive re-writes of the text and figures, and provided continuous
insights into interpretation of results and how to structure the manuscript. CAdS (Formal Analysis; Supervision; Validation;
Visualization; Writing – review & editing) trained and supervised FDR in microplankton light-microscopy qualitative and
quantitative analysis, performed nMDS, CA, and OMI niche analysis, guided interpretations of these results, and helped with
extensive re-writes of the text and figures. EA (Investigation; Formal Analysis; Writing – review & editing) and RT (Funding
acquisition; Investigation; Formal Analysis; Writing – review & editing) performed the analysis of carbonate system
parameters, nutrients, opal and chl-*a* and helped characterize the physical environments. EM (Investigation; Formal Analysis;
Writing – review & editing) carried out sampling and CTD deployment during the 2017 survey, and together with HG (Funding
acquisition; Writing – review & editing) provided insights into the interpretation of oceanographic results. All co-authors
provided key comments and editing of the final draft of the paper.

Competing interests

The authors declare no competing interests

References

Abril, G., Bouillon, S., Darchambeau, F., Teodoru, C., Marwick, T., Tamooh, F., Ochieng, F., Geeraert, N., Deirmendjian, L., Polsenaere, P., and Borges, A.: Technical note: large overestimation of pCO_2 calculated from pH and alkalinity in acidic, 675   organic-rich freshwaters, Biogeosciences, 12, 67-78, doi: 10.5194/bg-12-67-2015, 2015.

Alves-de-Souza C., González, M., and Iriarte, J.: Functional groups in marine phytoplankton assemblages dominated by diatoms in fjords of southern Chile, Journal of Plankton Research, 30(11), 1233-1243, doi: 10.1093/plankt/fbn079, 2008.

Alvites, D.: Variabilidad espacial y calcificación de las comunidades de cocolitofóridos en el sistema de afloramiento costero frente al Callao-Perú, Tesis de Maestro, Universidad Peruana Cayetano Heredia, 128 pp., 2016.

680   Bach, L., Riebesell, U., Gutowska, M., Federwisch, L., and Schulz, K.: A unifying concept of coccolithophore sensitivity to changing carbonate chemistry embedded in an ecological framework, Progress in Oceanography, 135, 125–138, doi: 10.1016/j.pocean.2015.04.012, 2015.

Baumann, K.-H., Andruleit, H., and Samtleben, C.: Coccolithophores in the Nordic Seas: comparison of living communities with surface sediment assemblages, Deep-Sea Research II, 47, 1743–1772, doi: 10.1016/S0967-0645(00)00005-9, 2000.

685   Beaufort, L., Couapel, M., Buchet, N., Claustre, H., and Goyet, C.: Calcite production by coccolithophores in the south east Pacific Ocean, Biogeosciences, 5(4), 1101–1117, doi:10.5194/bg-5-1101-2008, 2008.

Beaufort, L., Probert, I., de Garidel-Thoron, T., Bendif, E., Ruiz-Pino, D., Metzl, N., Goyet, C., Buchet, N., Coupel, P., Grelaud, M., Rost, B., Rickaby, R., and de Vargas, C.: Sensitivity of coccolithophores to carbonate chemistry and ocean acidification, Nature, 476(7358), 80–83, doi:10.1038/nature10295, 2011.

690   Bendif, E., Probert, I., Carmichael, M., Romac, S., Hagino, K., and de Vargas, C.: Genetic delineation between and within the widespread coccolithophore morpho-species *Emiliania huxleyi* and *Gephyrocapsa oceanica* (Haptophyta), Journal of Phycology, 50, 140–148, doi: 10.1111/jpy.12147, 2014.

Bendif, E., Probert, I., Díaz-Rosas, F., Thomas, D., van den Engh, G., Young, J., and von Dassow, P.: Recent reticulate evolution in the ecologically dominant lineage of coccolithophores, Frontiers in Microbiology, 7:784, 695   doi:10.3389/fmicb.2016.00784, 2016.

Bendif, E., Nevado, B., Wong, E., Hagino, K., Probert, I., Young, J., Rickaby, R., and Filatov, D.: Repeated species radiations in the recent evolution of the key marine phytoplankton lineage *Gephyrocapsa*, Nature communications, 10:4234, doi: 10.1038/s41467-019-12169-7, 2019.

Berge, G.: Discoloration of the sea due to *Coccolithus huxley* I "bloom", Sarsia, 6(1), 27–40, 700   doi:10.1080/00364827.1962.10410259, 1962.

Birkenes, E. and Braarud, T.: Phytoplankton in the Oslo fjord during a "*Coccolithus huxleyi*-summer", Avhandl. Norske Videnskaps - Akd. Oslo. I. Mat. Naturv. Klasse, 2, 1–23, 1952.

Bollmann, J., Cortés, M., Haidar, A., Brabec, B., Close, A., Hofmann, R., Palma, S., Tupas, L., and Thierstein, H.: Techniques for quantitative analyses of calcareous marine phytoplankton, Marine Micropaleontology, 44(3-4), 163–185, doi: 705   10.1016/S0377-8398(01)00040-8, 2002.

Broecker, W. and Clark, E.: Ratio of coccolith $CaCO_3$ to foraminifera $CaCO_3$ in late Holocene deep sea sediments, Paleoceanography, 24(3), 1–11, doi:10.1029/2009PA001731, 2009.

Brzezinski, M., Dickson, M., Nelson, D., and Sambrotto, R.: Ratios of Si, C and N uptake by microplankton in the Southern Ocean, Deep Sea Research Part II: Topical Studies in Oceanography, 50(3–4), 619–633, doi:10.1016/S0967-0645(02)00587- 710   8, 2003.

Cermeño, P., Lee, J.-B., Wyman, K., Schofield, O., and Falkowski, P: Competitive dynamics in two species of marine phytoplankton under non-equilibrium conditions, Marine Ecology Progress Series, 429, 1928, doi: 10.3354/meps09088, 2011.

Charalampopoulou, A., Poulton, A., Tyrrell, T., and Lucas, M.: Irradiance and pH affect coccolithophore community composition on a transect between the North Sea and the Arctic Ocean, Mar. Ecol. Prog. Ser., 431, 25–43, 715   doi:10.3354/meps09140, 2011.

Charalampopoulou, A., Poulton, A., Bakker, D., Lucas, M., Stinchcombe, M., and Tyrrell, T.: Environmental drivers of coccolithophore abundance and calcification across Drake Passage (Southern Ocean), Biogeosciences, 13, 5917–5935, doi: 10.5194/bg-13-5917-2016, 2016.

Cook, S., Jones, R., Vaillancourt, R., and Hallegraeff, G.: Genetic differentiation among Australian and southern ocean 720   populations of the ubiquitous coccolithophore *Emiliania huxleyi* (Haptophyta), Phycologia, 52, 368–374, doi: 10.2216/12- 111.1, 2013.

Corstjens, P., van der Kooij, A., Linschooten, C., Brouwers, G.-J., Westbroek, P., and Vrind-de Jong, E.: GPA, a calcium- binding protein in the coccolithophorid *Emiliania huxleyi* (Prymnesiophyceae), Journal of Phycology, 34, 622–630, 1998.

Cubillos, J., Wright, S., Nash, G., de Salas, M., Griffiths, B., Tilbrook, B., Poisson, A., and Hallegraeff, G.: Calcification 725   morphotypes of the coccolithophorid *Emiliania huxleyi* in the Southern Ocean: changes in 2001 to 2006 compared to historical data, Marine Ecology Progress Series, 348, 47–54, doi:10.3354/meps07058, 2007.

Cuevas, A., Tapia, F., Iriarte, J., González, H., Silva, N., and Vargas, C.: Interplay between freshwater discharge and oceanic waters modulates phytoplankton size-structure in fjords and channel systems of the Chilean Patagonia, Progress in Oceanography, 173, 103–113, doi: 10.1016/j.pocean.2019.02.012, 2019.

730   Cyronak, T., Schulz, K., and Jokiel, P.: The Omega myth: what really drives lower calcification rates in an acidifying ocean, ICES Journal of Marine Science, 73(3), 558–562, doi:10.1093/icesjms/fsv075, 2016.

Dávila, P., Figueroa, D., and Müller, E.: Freshwater input into the coastal ocean and its relation with the salinity distribution off austral Chile (35–55°S), Continental Shelf Research, 22(3), 521–534, doi:10.1016/S0278-4343(01)00072-3, 2002.

Dickson, A. and Millero, F.: A comparison of the equilibrium constants for the dissociation of carbonic acid in seawater media, Deep Sea Research Part A, Oceanographic Research Papers, 34(10), 1733–1743, doi:10.1016/0198-0149(87)90021-5, 1987.

Dolédec, S., Chessel, D., and Gimaret-Carpentier, C.: Niche separation in community analysis: A new method, Ecology, 81(10), 2914–2927, doi: 10.2307/177351, 2000.

Doney, S., Fabry, V., Feely, R., and Kleypas, J.: Ocean acidification: the other CO_2 problem, Annu. Rev. Mar. Sci., 1: 169–192, doi: 10.1146/annurev.marine.010908.163834, 2009.

Dray, S. and Dufour, A.: The ade4 package: implementing the duality diagram for ecologists. J. Stat. Softw, 22(4), 1–20, doi: 10.18637/jss.v022.i04, 2007.

Dufrene, M. and Legendre, P.: Species assemblages and indicator species: the need for a flexible asymmetrical approach, Ecol. Monogr., 67(3), 345–366, doi:10.2307/2963459, 1997.

Egge, E., Johannessen, T., Andersen, T., Eikrem, W., Bittner, L., Larsen, A., Sandaa, R., and Edvardsen, B.: Seasonal diversity and dynamics of haptophytes in the Skagerrak, Norway, explored by high-throughput sequencing, Mol. Ecol., 24(12), 3026–3042, doi:10.1111/mec.13160, 2015.

Erga, S.: Ecological studies on the phytoplankton of Boknafjorden, western Norway. 1. The effect of water exchange processes and environmental factors on temporal and vertical variability of biomass, Sarsia, 74(3), 161–176, doi:10.1080/00364827.1989.10413425, 1989.

Feely, R., Doney, S., and Cooley, S.: Ocean acidification: Present conditions and future changes in a high-CO_2 world, Oceanography, 22(4), 36–47, doi:10.5670/oceanog.2009.95, 2009.

Fernández, E., Marañón, E., Harbour, D., Kristiansen, S., and Heimdal, B.: Patterns of carbon and nitrogen uptake during blooms of *Emiliania huxleyi* in two Norwegian fjords, J. Plankton Res., 18(12), 2349–2366, doi:10.1093/plankt/18.12.2349, 1996.

Filatov, D.: Extreme Lewontin's paradox in ubiquitous marine phytoplankton species, Mol. Biol. Evol., 36(1), 4–14, doi: 10.1093/molbev/msy195, 2019.

Franco, A., Gruber, N., Frölicher, T., and Artman, L.: Contrasting impact of future CO_2 emission scenarios on the extent of $CaCO_3$ mineral undersaturation in the Humboldt Current System, J. Geophys. Res. Oceans, 123, 2018–2036, doi: 10.1002/2018JC013857, 2018.

Gafar, N., Eyre, B., and Schulz, K.: A conceptual model for projecting coccolithophorid growth, calcification and photosynthetic carbon fixation rates in response to global ocean change, Frontiers in Marine Science, 4, 433, doi: 10.3389/fmars.2017.00433, 2018.

Giraudeau, J., Monteiro, P., and Nikodemus, K.: Distribution and malformation of living coccolithophores in the northern Benguela upwelling system off Namibia, Marine Micropaleontology, 22, 93–110, doi: 10.1016/0377-8398(93)90005-I, 1993.

González, H., Castro, L., Daneri, G., Iriarte, J., Silva, N., Tapia, F., Teca, E., and Vargas, C.: Land-ocean gradient in haline stratification and its effects on plankton dynamics and trophic carbon fluxes in Chilean Patagonian fjords (47–50ºS), Progress in Oceanography, 119, 32–47, doi: 10.1016/j.pocean.2013.06.003, 2013.

Gran-Stadniczeñko, S., Šupraha, L., Egge, E., and Edvardsen, B.: Haptophyte diversity and vertical distribution explored by 18S and 28S ribosomal RNA gene metabarcoding and scanning electron microscopy, J. Eukaryot. Microbiol., 64(4), 514–532, doi:10.1111/jeu.12388, 2017.

Hagino, K., Bendif, E., Young, J., Kogame, K., Probert, I., Takano, Y., Horiguchi, T., de Vargas, C., and Okada, H.: New evidence for morphological and genetic variation in the cosmopolitan coccolithophore *Emiliania huxleyi* (Prymnesiophyceae) from the cox1b-atp4 genes, J. Phycol., 47(5), 1164–1176, doi:10.1111/j.1529-8817.2011.01053.x, 2011.

Hagino, K. and Okada, H.: Intra- and infra-specific morphological variation in selected coccolithophore species in the equatorial and subequatorial Pacific Ocean, Marine Micropaleontology, 58, 184–206, doi: 10.1016/j.marmicro.2005.11.001, 2006.

Hartin, C., Bond-Lamberty, B., Patel, P., and Mundra, A.: Ocean acidification over the next three centuries using a simple global climate carbon-cycle model: projections and sensitivities, Biogeosciences, 13, 4329–4342, 10.5194/bg-13-4329-2016, 2016.

Harvey, E., Bidle, K., and Johnson, M.: Consequences of strain variability and calcification in *Emiliania huxleyi* on microzooplankton grazing, Journal of Plankton Research, 37, 1137–1148, doi: 10.1093/plankt/fbv081, 2015.

Haunost, M., Riebesell, U., and Bach, L.: The calcium carbonate shell of *Emiliania huxleyi* provides limited protection against viral infection, Frontiers in Marine Science, 7, 530757, doi: 10.3389/fmars.2020.530757, 2020.

Henderiks, J., Winter, A., Elbrächter, M., Feistel, R., van der Plas, A., Nausch, G., and Barlow, R.: Environmental controls on *Emiliania huxleyi* morphotypes in the Benguela coastal upwelling system (SE Atlantic), Marine Ecology Progress Series, 448, 51–66, doi: 10.3354/meps09535, 2012.

Hernández, T., Bacher, C., Soudant, D., Belin, C., and Barillé, L.: Assessing phytoplankton realized niches using a French national phytoplankton monitoring network, Estuarine, Coastal and Shelf Science, 159, 15–27, doi: 10.1016/j.ecss.2015.03.010, 2015.

Hillebrand, H., Dürselen, C., Kirschtel, D., Pollingher, U., and Zohary, T.: Biovolume calculation for pelagic and benthic microalgae, J. Phycol., 35(2), 403–424, doi:10.1046/j.1529-8817.1999.3520403.x, 1999.

Hopkins, J., Henson, S., Poulton, A., and Balch, W.: Regional characteristics of the temporal variability in the global particulate inorganic carbon inventory, Global Biogeochemical Cycles, 33(11), 1328–1338, doi:10.1029/2019GB006300, 2019.

Iglesias-Rodriguez, D., Halloran, P., Rickaby, R., Hall, I., Colmenero-Hidalgo, E., Gittins, J., Green, D., Tyrrell, T., Gibbs, S., von Dassow, P., Rehm, E., Armbrust, V., and Boessenkool, K.: Phytoplankton calcification in a high-CO_2 world, Science, 320: 336–340, doi: 10.1126/science.1154122, 2008.

Jin, P., Ding, J., Xing, T., Riebesell, U., and Gao, K.: High levels of solar radiation offset impacts of ocean acidification on calcifying and non-calcifying strains of *Emiliania huxleyi*, Marine Ecology Progress Series, 568, 47–58, doi: 10.3354/meps12042, 2017.

800 Johns, Ch., Grubb, A., Nissimov, J., Natale, F., Knapp, V., Mui, A., Fredricks, H., Van Mooy, B., and Bidle, K.: The mutual interplay between calcification and coccolithovirus infection, Environmental microbiology, 21, 1896–1915, doi: 10.1111/1462-2920.14362, 2019.

Johnsen, S. and Bollmann, J.: Coccolith mass and morphology of different *Emiliania huxleyi* morphotypes: A critical examination using Canary Islands material, PLoS ONE, 15(3), e0230569, doi: 10.1371/journal.pone.0230569, 2020.

805 Jones, E., Chierici, M., Skjelvan, I., Norli, M., Børsheim, K., Lødemel, H., Sørensen, K., King, A., Lauvset, S., Jackson, K., de Lange, T., Johannsessen, T., and Mourgues, C.: Monitoring ocean acidification in Norwegian seas in 2018, Rapport, Miljødirektoratet, M-1417|2019, 2019.

Klaas, C. and Archer, D.: Association of sinking organic matter with various types of mineral ballast in the deep sea: Implications for the rain ratio, Global Biogeochemical Cycles, 16(4), 1116, doi:10.1029/2001GB001765, 2002.

810 Kottmeier, D., Rokitta, S., and Rost, B.: Acidification, not carbonation, is the major regulator of carbon fluxes in the coccolithophore *Emiliania huxleyi*, New Phytologist, 211, 126–137, 2016.

Kleypas, J., Feely, R., Fabry, V., Langdon, C., Sabine, C., and Robbins, L. Impacts of Ocean Acidification on Coral Reefs and Other Marine Calcifiers: A Guide for Future Research. Report of a workshop held 18–20 April 2005, St. Petersburg, FL, sponsored by NSF, NOAA, and the U.S. Geological Survey, 88 pp., 2006.

815 Kristiansen, S., Thingstad, F., van der Wal, P., Farbrot, T., and Skjoldal, E.: An *Emiliania huxleyi* dominated subsurface bloom in Samnangerfjorden, western Norway. Importance of hydrography and nutrients, Sarsia, 79(4), 357–368, doi:10.1080/00364827.1994.10413567, 1994.

Krueger-Hadfield, S., Balestreri, C., Schroeder, J., Highfield, A., Helaouët, P., Allum, J., Moate, R., Lohbeck, K., Miller, P., Riebesell, U., Reusch, T., Rickaby, R., Young, J., Hallegraeff, G., Brownlee, C., and Schroeder, D.: Genotyping an *Emiliania*
820 *huxleyi* (prymnesiophyceae) bloom event in the North Sea reveals evidence of asexual reproduction, Biogeosciences, 11, 5215–5234, doi: 10.5194/bg-11-5215-2014, 2014.

Langer, G. and Geisen, M.: Species-specific responses of calcifying algae to changing seawater carbonate chemistry, Geochemistry, Geophysics, Geosystems, 7, Q09006, doi: 10.1029/2005GC001227, 2006.

Langer, G., Nehrke, G., Probert, I., Ly, J., and Ziveri, P.: Strain-specific responses of *Emiliania huxleyi* to changing seawater
825 carbonate chemistry, Biogeosciences, 6, 2637–2646, doi: 10.5194/bg-6-2637-2009, 2009.

Langer, G., Probert, I., Nehrke, G., and Ziveri, P.: The morphological response of *Emiliania huxleyi* to seawater carbonate chemistry changes: an inter-strain comparison, J. Nannoplankton Res., 32(1), 29–34, ISSN: 1210-8049, 2011.

Leblanc, K., Quéguiner, B., Diaz, F., Cornet, V., Michel-Rodriguez, M., Durrieu de Madron, X., Bowler, C., Malviya, S., Thyssen, M., Grégori, G., Rembauville, M., Grosso, O., Poulain, J., de Vargas, C., Pujo-Pay, M., and Conan, P.:
830 Nanoplanktonic diatoms are globally overlooked but play a role in spring blooms and carbon export, Nature communications, 9, 953, doi: 10.1038/s41467-018-03376-9, 2018.

Legendre, P. and Legendre, L.: Numerical Ecology, 3rd English edition. Elsevier Science BV, Amsterdam, 1,006 pp., 2012.

McIntyre, A., Bé, A., and Roche, M.: Modern Pacific coccolithophorida: a paleontological thermometer, Trans. N. Y. Acad. Sci., 32(6), 720–731, doi: 10.1111/j.2164-0947.1970.tb02746.x, 1970.

835 Margalef, R.: Life-forms of phytoplankton as survival alternatives in an unstable environment, Oceanologica Acta, 1, 493–509, 1978.

Mehrbach, C., Culberson, C., Hawley, J., and Pytkowicx, R.: Measurement of the apparent dissociation constants of carbonic acid in seawater at atmospheric pressure, Limnol. Oceanogr., 18(6), 897–907, doi:10.4319/lo.1973.18.6.0897, 1973.

Mella-Flores, D., Machon, J., Contreras-Porcia, L., Mesa-Campbell, S., and von Dassow, P.: Differential responses of
840 *Emiliania huxleyi* (Haptophyta) strains to copper excess, Cryptogamie, Algologie, 39(4), 481–509, doi: 10.7872/crya/v39.iss4.2018.481, 2018.

Menden-Deuer, S. and Lessard, E.: Carbon to volume relationships for dinoflagellates, diatoms, and other protist plankton, Limnol. Oceanogr., 45(3), 569–579, doi: 10.4319/lo.2000.45.3.0569, 2000.

Menschel, E., González, H., and Giesecke, R.: Coastal-oceanic distribution gradient of coccolithophores and their role in the
845 carbonate flux of the upwelling system off Concepción, Chile (36°S), J. Plankton Res., 38(4), 798–817, doi: 10.1093/plankt/fbw037, 2016.

Menschel, E. and González, H.: Carbon and calcium carbonate export driven by appendicularian faecal pellets in the Humboldt current system off Chile, Scientific Reports, 9, 16501, doi: 10.1038/s41598-019-52469-y, 2019.

Meyer, J. and Riebesell, U.: Reviews and Syntheses: Responses of coccolithophores to ocean acidification: a meta-analysis,
850 Biogeosciences, 12(6), 1671–1682, doi:10.5194/bg-12-1671-2015, 2015.

Monteiro, F., Bach, L., Brownlee, C., Bown, P., Rickaby, R., Poulton, A., Tyrrell, T., Beaufort, L., Dutkiewicz, S., Gibbs, S., Gutowska, M., Lee, R., Riebesell, U., Young, J., and Ridgwell, A.: Why marine phytoplankton calcify, Science Advances, 2(7), e1501822, doi:10.1126/sciadv.1501822, 2016.

Müller, M., Trull, T., and Hallegraeff, G.: Differing responses of three Southern Ocean *Emiliania huxleyi* ecotypes to changing
855 seawater carbonate chemistry, Mar. Ecol. Prog. Ser., 531, 81–90, doi: 10.3354/meps11309, 2015.

Müller, M., Trull, T., and Hallegraeff, G.: Independence of nutrient limitation and carbon dioxide impacts on the Southern Ocean coccolithophore *Emiliania huxleyi*, The ISME Journal, 11, 1777– 1787, doi: 10.1038/ismej.2017.53, 2017.

Nejstgaard, J., Gismervik, I., and Solberg, P.: Feeding and reproduction by *Calanus finmarchicus*, and microzooplankton grazing during mesocosm blooms of diatoms and the coccolithophore *Emiliania huxleyi*, Marine Ecology Progress Series, 147,
860 197–217, 1997.

O'Brien, C., Peloquin, J., Vogt, M., Heinle, M., Gruber, N., Ajani, P., Andruleit, H., Arístegui, J., Beaufort, L., Estrada, M., Karentz, D., Kopczynska, E., Lee, R., Poulton, A., Pritchard, T., and Widdicombe, C.: Global marine plankton functional type biomass distributions: coccolithophores, Earth Syst. Sci. Data, 5, 259–276, doi:10.5194/essd-5-259-2013, 2013.

Oksanen, J., Kindt, R., Legendre, P., O'Hara, B., and Stevens, H.: The vegan package, Community Ecology Package, 10, 631–
865 637, 2007.

Paasche, E. and Kristiansen, S.: Ammonium regeneration by microzooplankton in the Oslofjord, Mar. Biol., 69(1), 55–63, doi:10.1007/BF00396961, 1982.

Paredes, M., Montecino, V., Anic, V., Egaña, M., and Guzmán, L.: Diatoms and dinoflagellates macroscopic regularities shaped by intrinsic physical forcing variability in Patagonian and Fuegian fjords and channels (48º–56ºS), Progress in
870   Oceanography, 129, 85–97, doi: 10.1016/j.pocean.2014.07.002, 2014.

Passow, U. and Carlson, C.: The biological pump in a high CO_2 world, Mar. Ecol. Prog. Ser., 470, 249–271, doi:10.3354/meps09985, 2012.

Paul, A. and Bach, L.: Universal response pattern of phytoplankton growth rates to increasing CO_2, New Phytologist, 228, 1710–1716, doi: 10.1111/nph.16806, 2020.

875   Pierrot, D., Lewis, E., and Wallace, D. 2006. MS Excel Program Developed for CO2 System Calculations. ORNL/CDIAC-105a. Carbon Dioxide Information Analysis Center, Oak Ridge National Laboratory, U.S. Department of Energy, Oak Ridge, Tennessee. doi: 10.3334/CDIAC/otg.CO2SYS_XLS_CDIAC105a.

Poulton, A., Young, J., Bates, N., and Balch, W.: Biometry of detached *Emiliania huxleyi* coccoliths along the Patagonian Shelf, Mar. Ecol. Prog. Ser., 443, 1–17, doi:10.3354/meps09445, 2011.

880   Poulton, A., Painter, S., Young, J., Bates, N., Bowler, B., Drapeau, D., Lyczsckowski, E., and Balch, W.: The 2008 *Emiliania huxleyi* bloom along the Patagonian Shelf: Ecology, biogeochemistry, and cellular calcification, Global Biogeochemical Cycles, 27(4), 1023–1033, doi:10.1002/2013GB004641, 2013.

R Core Team (2019). R: A language and environment for statistical computing. R Foundation for Statistical Computing, Vienna, Austria, URL http://www.R-project.org/.

885   Read, B., Kegel, J., Klute, M., Kuo, A., Lefebvre, S., Maumus, F., Mayer, Ch., Miller, J., Monier, A., Salamov, A., Young, J., Aguilar, M., Claverie, J.-M-, Frickenhaus, S., Gonzalez, K., Herman, E., Lin, Y.-Ch., Napier, J., Ogata, H., Sarno, A., Shmutz, J., Schroeder, D., de Vargas, C., Verret, F., von Dassow, P., Valentin, K., Van de Peer, Y., Wheeler, G., Emiliania huxleyi Annotation Consortium, Dacks, J., Delwiche, Ch., Dyhrman, S., Glöckner, G., John, U., Richards, T., Worden, A., Zhang, X., and Grigoriev, I.: Pan genome of the phytoplankton *Emiliania* underpins its global distribution, Nature, 499, 209–213, doi:
890   10.1038/nature12221, 2013.

Rickaby, R., Hermoso, M., Lee, R., Rae, B., Heureux, A., Balestreri, C., Chakravarti, L., Schroeder, D., and Brownlee, C.: Environmental carbonate chemistry selects for phenotype of recently isolated strains of *Emiliania huxleyi*, Deep-Sea Research II, 127, 2840, doi: 10.1016/j.dsr2.2016.02.010, 2016.

Riebesell, U., Bach, L., Bellerby, R., Monsalve, R., Boxhammer, T., Czerny, J., Larsen, A., Ludwig, A., and Schulz, K.:
895   Competitive fitness of a predominant pelagic calcifier impaired by ocean acidification, Nature Geosci., 10, 19–23, doi: 10.1038/ngeo2854, 2017.

Rivero-Calle, S., Gnanadesikan, A., Del Castillo, C., Balch, W., and Guikema, S.: Multidecadal increase in North Atlantic coccolithophores and the potential role of rising CO_2, Science, 350(6267), 1533–1537, doi:10.1126/science.aaa8026, 2015.

Rokitta, S. and Rost, B.: Effects of CO_2 and their modulation by light in the life-cycle stages of the coccolithophore *Emiliania*

900   *huxleyi*, Limnology and Oceanography, 57, 607–618, doi: 10.4319/lo.2012.57.2.0607, 2012.

Saavedra-Pellitero, M., Baumann, K., Flores, J., and Gersonde, R.: Biogeographic distribution of living coccolithophores in the Pacific sector of the Southern Ocean, Marine Micropaleontology, 109, 1–20, doi: 10.1016/j.marmicro.2014.03.003, 2014.

Saavedra-Pellitero, M., Baumann, K., Fuertes, M., Schulz, H., Marcon, Y., Vollmar, N., Flores, J., and Lamy, F.: Calcification and latitudinal distribution of extant coccolithophores across the Drake Passage during late austral summer 2016,

905   Biogeosciences, 16, 3679–3702, doi: 10.5194/bg-16-3679-2019, 2019.

Samtleben, C., Schäfer, P., Andruleit, H., Baumann, A., Baumann, K., Kohly, A., Matthiessen, J., Schröder-Ritzrau, A., and 'Synpal' Working Group: Plankton in the Norwegian-Greenland Sea: from living communities to sediment assemblages - an actualistic approach, Geol. Rundsch., 84(1), 108–136, doi: 10.1007/BF00192245, 1995.

Schlitzer, R., Ocean Data View, URL https://odv.awi.de/, 2018.

910   Schroeder, D., Biggi, G., Hall, M., Davy, J., Martínez, J., Richardson, A., Malin, G., and Wilson, W.: A genetic marker to separate *Emiliania huxleyi* (Prymnesiophyceae) morphotypes, Journal of Phycology, 41, 874–879, doi: 10.1111/j.1529-8817.2005.04188.x, 2005.

Sicko-Goad, L., Schelske, C., and Stoermer, E.: Estimation of intracellular carbon and silica content of diatoms from natural assemblages using morphometric techniques, Limnol. Oceanogr., 29(6), 1170–1178, doi: 10.4319/lo.1984.29.6.1170, 1984.

915   Sievers, H. and Silva, N.: Water masses and circulation in austral Chilean channels and fjords, in Progress in the oceanographic knowledge of Chilean interior waters, from Puerto Montt to Cape Horn, edited by: Silva, N. and Palma, S., Comité Oceanográfico Nacional, Pontificia Universidad Católica de Valparaiso, 53–58, 2008.

Smith, H., Tyrrell, T., Charalampopoulou, A., Dumousseaud, C., Legge, O., Birchenough, S., Pettit, L., Garley, R., Hartman, S., Hartman, M., Sagoo, N., Daniels, C., Achterberg, E., and Hydes, D.: Predominance of heavily calcified coccolithophores

920   at low $CaCO_3$ saturation during winter in the Bay of Biscay, Proc. Natl. Acad. Sci. U.S.A., 109(23), 8845–8849, doi:10.1073/pnas.1117508109, 2012.

Smith, H., Poulton, A., Garley, R., Hopkins, J., Lubelczyk, L., Drapeau, D., Rauschenberg, S., Twining, B., Bates, N., and Balch, W.: The influence of environmental variability on the biogeography of coccolithophores and diatoms in the Great Calcite Belt, Biogeosciences, 14, 4905–4925, doi: 10.5194/bg-14-4905-2017, 2017.

925   Strom, S., Bright, K., Fredrickson, K., and Cooney, E.: Phytoplankton defenses: Do *Emiliania huxleyi* coccoliths protect against microzooplankton predators? Limnology and Oceanography, 63, 617–627, doi: 10.1002/lno.10655, 2018.

Takahashi, T., Sutherland, S., Chipman, D., Goddard, J., Ho, Ch., Newberger, T., Sweeney, C., and Munro, D.: Climatological distributions of pH, pCO_2, total CO_2, alkalinity, and $CaCO_3$ saturation in the global surface ocean, and temporal changes at selected locations, Marine Chemistry, 164, 95–125, doi: 10.1016/j.marchem.2014.06.004, 2014.

930   Taylor, A., Brownlee, C., and Wheeler, G.: Coccolithophore cell biology: Chalking up progress, Annu. Rev. Mar. Sci., 9(1), 283–310, doi:10.1146/annurev-marine-122414-034032, 2017.

Torres, R., Pantoja, S., Harada, N., González, H., Daneri, G., Frangopulos, M., Rutllant, J., Duarte, C., Rúiz-Halpern, S., Mayol, E., and Fukasawa, M.: Air-sea CO_2 fluxes along the coast of Chile: From CO_2 outgassing in central northern upwelling waters to CO_2 uptake in southern Patagonian fjords, J. Geophys. Res., 116(C9), C09006, doi: 10.1029/2010JC006344, 2011.

935 Torres, R., Silva, N., Reid, B., and Frangopulos, M.: Silicic acid enrichment of subantarctic surface water from continental inputs along the Patagonian archipelago interior sea (41–56°S), Progress in Oceanography, 129, 50–61, doi: 10.1016/j.pocean.2014.09.008, 2014.

Torres, R., Reid, B., Frangopulos, M., Alarcón E., Márquez M., Haussermann, V., Försterra, G., Pizarro, G., Iriarte, J., and Gonzalez, H.: Freshwater runoff effects on the production of biogenic silicate and chlorophyll-a in western Patagonia

940 archipelago (50-51°S), Estuarine, Coastal and Shelf Science, 241, 106597, doi: 10.1016/j.ecss.2020.106597, 2020.

Tynan, E., Tyrrell, T., and Achterberg, E.: Controls on the seasonal variability of calcium carbonate saturation states in the Atlantic gateway to the Arctic Ocean, Marine Chemistry, 158, 1–9, doi: 10.1016/j.marchem.2013.10.010, 2014.

Tyrrell, T. and Merico, A.: *Emiliania huxleyi*: bloom observation and the conditions that induce them, in Coccolithophores, edited by: Thierstein, H. and Young, J., Springer, Berlin, Heidelberg, Germany, 75–97, doi: 10.1007/978-3-662-06278-4_4,

945 2004.

Utermöhl, H.: Vervollkommnung der quantitativen phytoplankton-methodik, Mitteilungen. Internationale Vereinigung für theoretische und angewandte Limnologie, 9, 1–38, 1958.

van Bleijswijk, J., van der Wal, P., Kempers, R., Veldhuis, M., Young, J., Muyzer, G., Vrind-de Jong, E., and Westbroek, P.: Distribution of two types of *Emiliania huxleyi* (Prymnesiophyceae) in the northeast Atlantic region as determined by

950 immunofluorescence and coccolith morphology, J. Phycol., 27(5), 566–570, doi: 10.1111/j.0022-3646.1991.00566.x, 1991.

Vivanco, X. and Seguel, M.: Manual Técnico – Curso teórico-práctico para el muestreo, identificación y enumeración de *Alexandrium catenella* y otros taxa nocivos, Instituto de Fomento Pesquero, Puerto Montt, Chile, https://www.ifop.cl/marearoja/wp-content/uploads/sites/2/2016/07/Manual_Tecnico_curso_Marzo_2009-mod.pdf, 2009.

von Dassow, P., John, U., Ogata, H., Probert, I., Bendif, E., Kegel, J., Audic, S., Wincker, P., Da Silva, C., Claverie, J., Doney,

955 S., Glover, D., Mella, D., Herrera, Y., Lescot, M., Garet-Delmas, M., and de Vargas, C.: Life-cycle modification in open oceans accounts for genome variability in a cosmopolitan phytoplankton, The ISME Journal, 9, 1365–1377, doi: 10.1038/ismej.2014.221, 2015.

von Dassow, P., Díaz-Rosas, F., Bendif, E., Gaitán-Espitia, J., Mella-Flores, D., Rokitta, S., John, U., and Torres, R.: Over-calcified forms of the coccolithophore *Emiliania huxleyi* in high-CO_2 waters are not preadapted to ocean acidification,

960 Biogeosciences, 15(5), 1515–1534, doi:10.5194/bg-15-1515-2018, 2018.

Young, J. and Westbroek, P.: Genotypic variation in the coccolithophorid species *Emiliania huxleyi*, Marine Micropaleontology, 18(1–2), 5–23, doi:10.1016/0377-8398(91)90004-P, 1991.

Young, J.: Variation in *Emiliania huxleyi* coccolith morphology in samples from the Norwegian EHUX experiment, 1992, Sarsia, 79(4), 417–425, doi:10.1080/00364827.1994.10413573, 1994.

965   Young, J., Geisen, M., Cros, L., Kleijne, A., Sprengel, C., Probert, I., and Ostergaard, J.: A guide to extant coccolithophore taxonomy, Journal of Nannoplankton Research Special Issue, (1), 1–125, ISSN:1210-8049, 2003.

Young, J., Poulton, A., and Tyrrell, T.: Morphology of *Emiliania huxleyi* coccoliths on the northwestern European shelf – is there an influence of carbonate chemistry? Biogeosciences, 11, 4771–4782, doi:10.5194/bg-11-4771-2014, 2014.

Zhang, Y., Fu, F., Hutchins, D., and Gao, K.: Combined effects of CO_2 level, light intensity, and nutrient availability on the
970   coccolithophore *Emiliania huxleyi*, Hydrobiologia, 842, 127-141, doi: 10.1007/s10750-019-04031-0, 2019.

Zingone, A., Sarno, D., Siano, R., and Marino, D.: The importance and distinctiveness of small-sized phytoplankton in the Magellan Straits, Polar Biol., 34(9), 1269–1284, doi: 10.1007/s00300-010-0937-2, 2011.

Ziveri, P., Bernardi, B., Baumann, K.-H., Stoll, H., and Mortyn, G.: Sinking of coccolith carbonate and potential contribution to organic carbon ballasting in the deep ocean, Deep-Sea Research, 54, 659–675, doi: 10.1016/j.dsr2.2007.01.006, 2007.

975   Zondervan, I., Zeebe, R., Rost, B., and Riebesell, U.: Decreasing marine biogenic calcification: A negative feedback on rising atmospheric pCO2, Global Biogeochem. Cycles, 15(2), 507–516, doi: 10.1029/2000GB001321, 2001.